INFLUENCE OF SALINOUS SOLUTIONS IN THE PRESSURE AND VOLUME MODULATIONS OF THE INTRACRANIAL CAVITY

A Thesis

by

MARIANA CEBALLOS

Submitted to the Office of Graduate Studies of
Texas A&M University
in partial fulfillment of the requirements for the degree of

MASTER OF SCIENCE

August 2011

Major Subject: Mechanical Engineering

INFLUENCE OF SALINOUS SOLUTIONS IN THE PRESSURE AND VOLUME MODULATIONS OF THE INTRACRANIAL CAVITY

A Thesis

by

MARIANA CEBALLOS

Submitted to the Office of Graduate Studies of
Texas A&M University
in partial fulfillment of the requirements for the degree of

MASTER OF SCIENCE

Approved by:

Co-Chairs of Committee,	Hong Liang
	Sai Lau
Committee Member,	Matthew Sachs
Head of Department,	Dennis O'Neal

August 2011

Major Subject: Mechanical Engineering

ABSTRACT

Influence of Salinous Solutions in the Pressure and Volume Modulations of the Intracranial Cavity. (August 2011)

Mariana Ceballos, B.S., Florida International University

Co-Chairs of Advisory Committee: Dr. Hong Liang
Dr. Sai Lau

Following a head concussion the intracranial pressure increases due to the impact, which cannot be adequately relieved because of the stiffness of the skull. Popular strategies aimed at decompressing the head consist in the administration of osmotic agents and skull removal.

The mechanical properties of bone can be affected by the administration of different solutions. If the malleability of skull is influenced by the osmotic agents that are administered to the patient then the pressure and volume in the intracranial cavity can also be modified following the treatment. In this thesis research, we hypothesize ***that administered osmotic agents can influence the mechanical properties of the skull, which can also impact the volume the cavity can hold and subsequently the pressure in the head.***

This premise was tested by modifying existing mathematical models compiled through two general MATLAB® codes that allow the computation of a non-symbolic differential-algebraic initial value problem. Three main features were changed in comparison to current models: the skull's influence on the pressure and volume

modulation was tested (inputs were obtained from skull tested under different solutions); pulsatile flow was accounted for on the creation and movement of cerebrospinal fluid; and the input on the mechanical behavior of the cranial vessels was accounted for through previously published continuum-mechanics vessel-behavior models. To complete the model, materials and mechanical properties were obtained through laboratory experiments as well as data collection from existing literature.

From our bone test we were able to conclude that there are different factors that affect the mechanical properties of bone in various degrees. There is a mild statistical correlation (p-value ≥ 0.05) between the mechanical properties of bone obtained from different regions of the skull samples (2-14mm) and the DPBS and hDPBS solutions. Additionally there is a strong statistical difference (p-value ≤ 0.05) between the mechanical properties obtained from cross head speed (0.02, 0.002, & 0.004 (mm/s)) and solution variation (DI, DPBS and hDPBS). Finally, we were able to see that there seems to be a correlation between the mechanical properties of bone, the solution treatments and hypertension; although more test need to be developed to affirm this premise since our results are preliminary.

DEDICATION

I dedicate my thesis to my grandparents who, through hard work, ensured a better life for the generations to come.

ACKNOWLEDGEMENTS

I would like to thank my committee chair, Dr. Liang, for her management of my research studies. My committee co-chair, Dr. Lau, for promoting research by bestowing studying opportunities for students and Dr. Sachs for aiding in my presentation rehearsals and thesis editing.

I also want to thank Mexico, my home country, and the Leo Rowe Fund for promoting research through national and international research grants. I want to thank my family because they have supported me through my entire student facet and Luis Eduardo Peternell Altamira for being a great partner and friend.

NOMENCLATURE AND ABBREVIATIONS

a	Final radius
Coeff	Coefficient
Conc	Concentration
Cond	Conductivity
CPP	Cerebral Perfusion Pressure
CVS	Cardiovascular
d	Diameter
D	Diameter
Depol	Depolarization
DI	Dionized water
DPBS	Diphosphate-Buffered Saline
E	Young's modulus
H	Height
Hct	Hematocrit
hPBS	Hyperosmolar Diphosphate-Buffered Saline
HR	Heart Rate
HTS	Hypertonic Saline
ICP	Intracranial Pressure
P	Pressure
R	Resistance

SPT	Small Punch Test
Sys	Organ System
TBI	Traumatic Brain Injury
Trans	Transport
V	Volume
ε	Strain
μ	Viscosity
π	Tissue Pressure
σ_{pl}	Peak stress

TABLE OF CONTENTS

Page

Page

CHAPTER

LIST OF FIGURES

Page

Page

LIST OF TABLES

CHAPTER I

INTRODUCTION

The relationship between hypertension and the skull rarely gets highlighted. It is important to understand how the bone interfaces with the intracranial cavity and how it reacts on the onset and treatment of hypertension, because this information will aid in the understanding of intracranial pressure (ICP).

In certain cases the skull cannot be used as a consideration in mathematical models of traumatic brain injury and its treatments because the knowledge base for the skull is incomplete. In order to improve the knowledge base about the skull and its relationship to the intracranial cavity we perform the following investigation which is organized as follows: The first portion of this chapter will briefly review common concepts for the study of mammalian biological systems and the condition studied in this investigation, Traumatic Brain Injury (TBI). The second section introduces the mechanical testing of bone and the analytical and theoretical aspects that are implemented in the analysis of bone. The third portion of this chapter will discuss the mathematical and biological models that have been developed, and are being developed, to study the influence that hyperosmolar[1] solutions have on the body.

This thesis follows the style of *Annual Review of Biomedical Engineering.*

[1] Hyperosmolar solutions or hypertonic solutions are solutions with a high solute content that are aimed at reducing edema in the patient (1). Hyperosmolar NaCl solutions were used by Dr. Wolf to test his mathematical model (2).

1.1. Regulation, injury and the restoration of activity in a biological system

Biological systems require a set of stable parameters like temperature, pressure, and concentration of substances to sustain life (3). The body's capability to uphold this range of values that bolster biological functions is called homeostasis (3; 4).

Homeostasis is maintained through a set of organ systems which work as a unit to maintain biological functions (3). In the human body, there are eleven main organ systems: circulatory, digestive, endocrine, integumentary, immune, skeletal, muscular, nervous, reproductive, respiratory, and urinary (3). This thesis will mainly focus on the study of the circulatory system and the skeletal system.

The circulatory system is comprised of the vessels, the heart, and the blood (3). It aids in the distribution of nutrients, water, gases, and other substances, and in the removal of metabolic wastes (5). The circulatory system regulates the pressure and volume of the whole body with the aid of the other organ systems to maintain homeostasis.

For example, the kidneys and hormonal signals are part of the vast regulation of vasoconstriction and dilation (e.g. natriuretic peptides and agiotensin II influence kidney ion excretion), which aid in the easing of pressure loads that damaged hearts can no longer bear (4). Other less common, and non-efficient, ways of coping with change in pressure or volume of fluid to maintain homeostasis might include an enlargement of the heart (6) and thickening of the skull (7).

The circulatory system can be compromised from several pathological conditions and toxins. Its impairment can be critical to the body because it can affect the blood supply and quality of the blood delivered to the organs and systems.

1.1.1. Injury

After an initial homeostatic upset of a biological system there are several stages that follow which are aimed at restoring homeostasis in the organism. The first response following an upset of the system is the inflammatory response (8). The inflammatory response is the cascade of events that involve the activation of immune cells, capillary leakage, increase of endothelial cell activity, dilation of the tissue, and other events that occur as a consequence of injury, disease, or other pathological condition (8; 9).

Inflammation can be beneficial to the body and help the system heal, it can also destroy tissues and endanger the organism (9). Inflammation can be acute or chronic. Acute inflammation lasts for a couple of days and involves the previously described processes(9). Chronic inflammation can last years (or an extended period of time) and deteriorates the tissues due the excessive inflammation, repair processes, and self-destruction of the organs. Examples of this inflammation are atherosclerosis, inflammatory bowel disease (9), and possibly Alzheimer's (10).

1.1.2. Traumatic Brain Injury (TBI)

Disruption of homeostasis by injury to the brain is often referred to as Traumatic Brain Injury, or TBI. TBI can cause two types of injury, initial or primary injury, which are the main trauma to the head that can be caused by several reasons (Figure 1) and injury that happens after the initial trauma (secondary injury). Primary injury can have grave

consequences such as permanent disfigurement, impairment of mental abilities, and death. However, in most cases the real danger of primary injury is its creation of secondary injury.

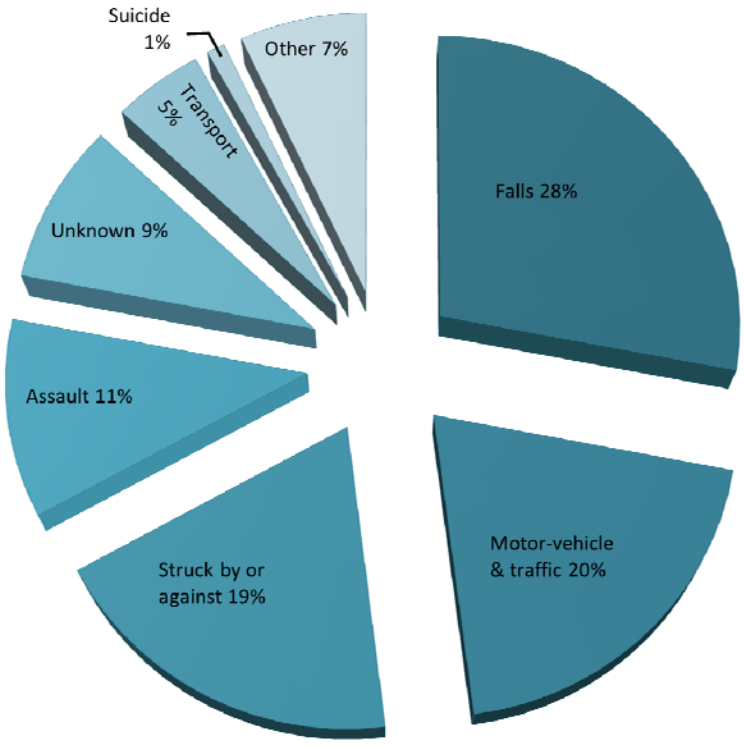

Figure 1 Major causes of Traumatic Brain Injury (11; 12).

Secondary injury can be caused by delayed tissue death or as a result of enzymatic and hypoxic processes (low oxygen supply) caused by the initial trauma (13). Secondary injury can also cause the creation of pores in the lipid bilayer which creates a misbalance in the ion concentrations in the cell plasma such as potassium, intracellular

sodium, chloride, and calcium levels (14). This non-homeostatic ion level can cause apoptosis and edema (14). Figure 2 shows some examples of primary injury and secondary injury.

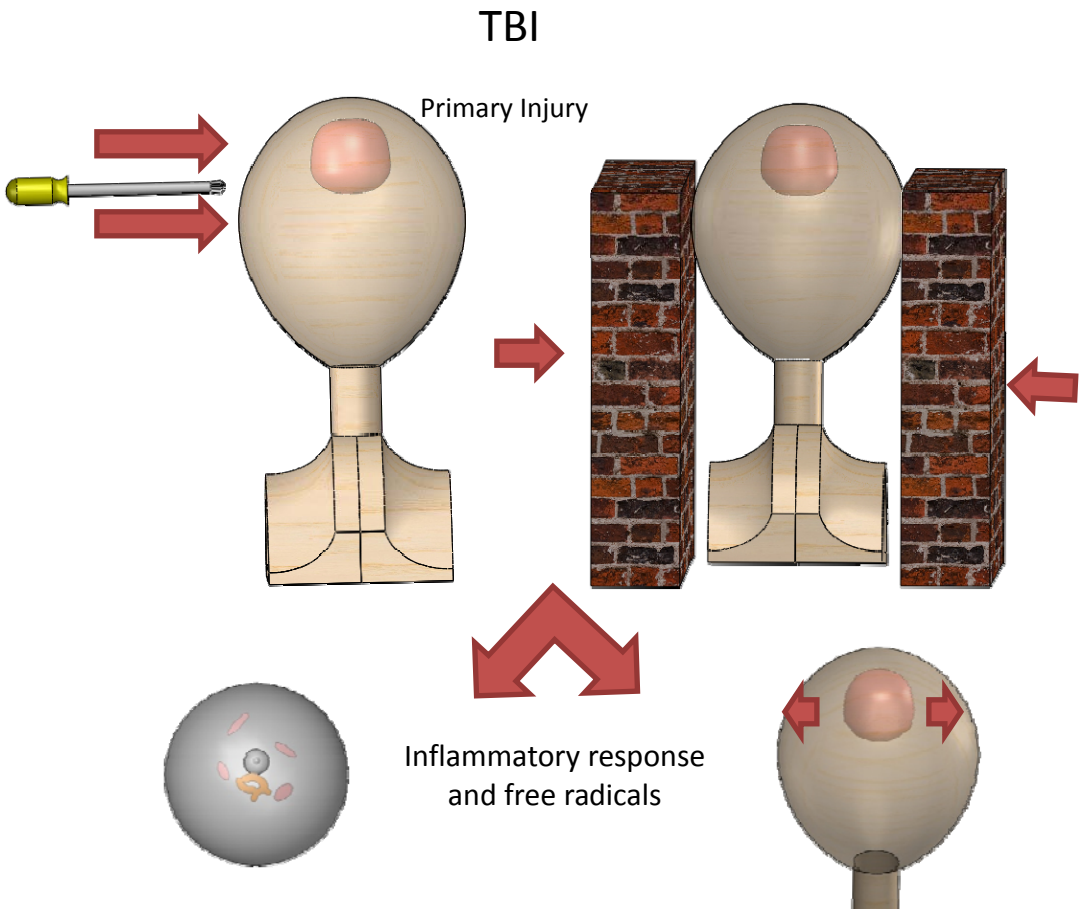

Figure 2 Traumatic Brain Injury.

There are an estimated 1.6-3 million TBI cases per year in the United States (14; 15). Patients that experience persistent and elevated pressure as a result of trauma

usually do not obtain a good prognosis (16). There is a real need in hospitals to lower the pressure of these patients in a timely manner since it has been noted that intracranial pressure above 20mmHg has been statistically correlated with a bad prognosis (17; 18).

The brain, which is surrounded by a solid skull, has a gel-like consistency and is embedded in fluid (18; 19), making an initial brain injury dangerous since skull stiffness concentrates the force applied (20). The injury, prognosis, and incidence of TBI make it a topic which needs to be researched in more depth. Nevertheless, there have been some interesting developments regarding the study of TBI in recent years. For example, while the rat is a well-known model for the study of TBI, swine is considered to be a better model for the study of this condition (14). Swine exhibits a traumatic injury response similar to the human and is now being used to study TBI (21).

Drug-based treatments that rely on osmosis and skull removal are the methods of choice for physicians treating TBI (22). But ICP as a result of TBI is a complicated condition, and no completely satisfactory treatment has yet been found since there are side effects for the used treatments such as hyperkalemia and hypernatremia (23; 24). Because these treatments are not completely effective we need to search for better ones. As we search for better treatments it is important to pinpoint what is effective and not in the current remedies. Therefore, in these studies we designed a computer code that can be used to analyze current and future treatments.

1.2. Mechanical evaluation and interpretation

Head testing for swine has been limited to the mandible test (25). The cranium mechanical test in swine is important in order to better understand the implications and

surroundings involved in traumatic brain injury. Better and more analysis are needed for swine bone, specifically of the skull. Bone cannot be analyzed and tested as a simple solid. It is compressible[2], anisotropic[3] (27), and viscoelastic[4] (28). Hooke's law[5] cannot be immediately applied to its analysis because of the compressibility[2] and anisotropy[3] of the material. Moreover, bone differs in its properties among close samples due to the small differences in constitution, in unit structure[6], and the failure of those structures (29); therefore small volumes of samples need to be tested.

1.2.1. Cellular solids

Cellular solids are solids with small compartments—or cells—that can be compressed through the collapse of their unit structures[6]. The small cells of these materials are arranged in two dimensional or three dimensional configurations (Figure 3) (26). These micro compartments are connected to each other in a partially or fully covered structures, consequently named open or closed cell foams (26).

---

[2] Compressible: the unit structures of bone and other cellular solids fail under compressible loads following a similar pattern of linear elasticity, plateau and densification (described in section 1.2.1). Overall the compression collapses the unit structure of the material, but produces a small spreading of the material in the lateral direction. It has been cited that cellular solids have a ration of 0.04 in lateral spread to axial compression (26).

[3] Anisotropy: the material displays different mechanical behavior along different directions.

[4] Viscoelasticity: the material stress-strain behavior depends on the rate of loading.

[5] Hooke's Law: metals and other common materials deform in following the prescribed mathematical relationship $\sigma=E\varepsilon$ where σ represents the stress, E the Young's modulus and ε the engineering strain (28).

[6] Unit Structure: cellular solids are characterized by structures that resemble cells, for example the cells in the corks. These structures are composed of smaller solid filaments or struts. Because this thesis includes other biological terms, the use of the term cellular structure was substituted for unit structure. After all, the cellular structure was the unit of the analysis and is the basis for the cellular behavior which gives bone most of its mechanical characteristic properties (26).

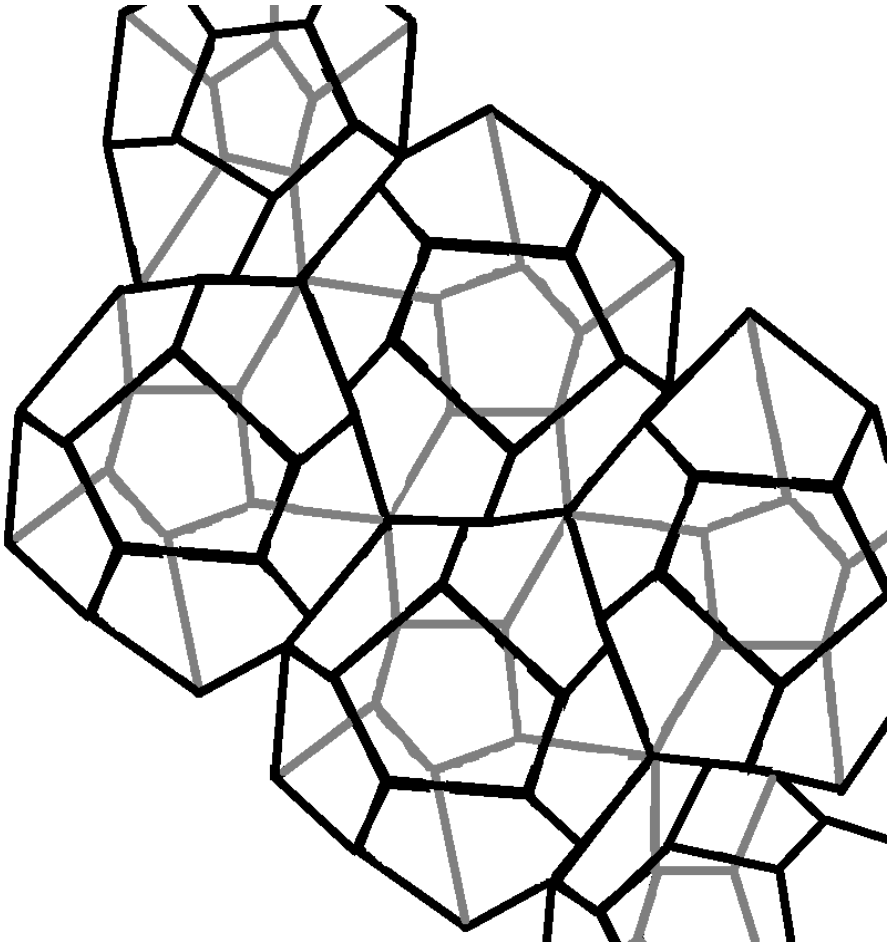

Figure 3 Three dimensional and open cell structure (struts are connected in an open arrangement) often found in cellular solids.

Bone also displays micro compartments and is very compressible; therefore bone can be described as a cellular solid. Density is important in cellular solids because it strongly influences other mechanical properties such as the Young's modulus (26). The density, the cellular arrangement, and material which form the struts[6] are the most important factors that determine the mechanical properties of cellular solids (30).

Mechanically, cellular solids behave similarly under compressive loads. They display three distinct phases in their load compression curves: a linear elastic region; a plateau phase, in which there is a relative large displacement for the given load; and

finally, after a large compaction of the cells, there is a densification phase (31; 32). Bone, as can be observed in the results section, displays the distinct mechanical behavior of cellular solids as well.

1.2.2. Bone

Bone is part of the skeletal system. The purpose for the skeletal system is to protect the internal structures, provide mobility for the body, serve as a hemopoitic locus, and support other tissues (33). Bone is composed mainly of water, hydroxyapatite, collagen, non-collagenous proteins, and cells (34). Bone develops into specific shapes such as long (e.g. arms and clavicles), flat (e.g. pelvis and skull), and short/irregular (vertebra and sternum) (28; 33).

Bones have an exterior more compact structure called cortical bone, and an interior medulla or cancellous bone (29). Compact bone has microscopic pores and is denser than cancellous bone (34; 35). Both have the same main organizational entity, the osteon (~150μm in diameter and ~1-2 cm in length), which can vary in morphology depending on the class of bone (36).

Bone behaves differently than other tissues when homeostasis is disrupted, because it can recover the use of function to nearly 100% through regulated cell behavior (8). Bone continuously grows and remodels to meet the demands it is subjected. Bone homeostasis is based on a delicate balance of bone growth and absorption, which is controlled by the osteoblast and osteoclast cells (36-40).

1.2.3. Bone mechanical behavior

The characteristics of bone in a macroscopic level (its pore size, density, strut characteristics, etc...) are determined by its use. Modifications happen during healing or remodeling and aid in making resistant structures that withstand the load the bone is subjected to (41-46). It is also important to mention that there is a significant variability between various characteristics of the bone in areas of the body (28) and among species (28).

There is also difference in the mechanical properties of bones treated with certain solutions. For example, Fluoride has been used for years to boost bone mass (47). Another substance that has known to affect the mechanical properties of bone is sodium chloride (salt). Salt can cause bone absorption (48), and therefore is one substance can decrease the strength of bone *in-vivo* (49). *In-vitro* modification of the mechanical properties of bone has never been positively proven prior to this research.

Finally, because bone is composed of ductile and elastic materials, the plateau failure is not as simple as other materials with a high level of elastic behavior. The elastic components in the material bestow special mechanical characteristics when tested due to the movement of each of the collagen fibers. These elaborate constitution makes bone mechanical properties dependent on the strain rate (or cross head speed[7]) used to test the material (28; 50; 51).

[7]Cross head speed: The speed at which the metallic arm of the test (cross head portion of the compressive test) is lowered in the experiment. This speed can be related to the strain rate.

1.2.4. Characterization of biological materials

Characterization of biological materials can determine the behavior of the material under physiological and non-physiological loading. There are different ways that materials can be characterized; mechanically, thermally, electrically, and chemically, among other characterizations (8).

Hard tissue e.g., bone, cartilage, horns and soft tissue e.g., skin, muscle, organs are often tested differently and the results analyzed in a different manner. This is because the properties of both are very different. For example the behavior of soft tissue vessels often gets recreated by the use of Fung's strain energy equation, which can recreate the behavior of soft tissue using concepts of continuum mechanics (52). Bone follows the behavior of other cellular solids such as foamed metals and polymers.

There are four common types of mechanical testing machines used for the characterization of bones (28). Single-axis machines, which are made of one axis, can be used for compressive, tensile, three-point bending test, and other popular tests (28). Multi-axis machines are used to resemble physiological forces, and are valuable in the test of spines because they have a rotary actuator that can simulate complicated loads (28).

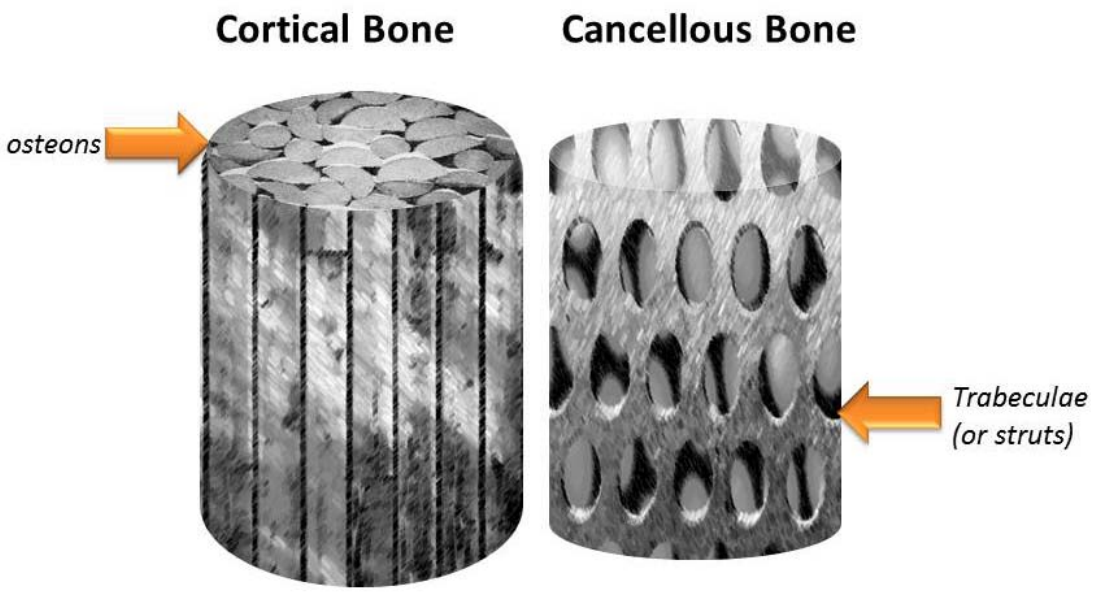

Figure 4 Bone and its main components.

Micromechanical testing machines allow the testing of parts of the unit structure of bone, such as the osteons and trabeculae (Figure 4). Hardness and indentation machines allow a complex characterization of bone because the load is a combination of shear and compressive forces (28). There are several micro hardness indentation tests which allow the characterization of the bone, including the unit structure (in this case that structure is 100 μm), such as the Small Punch Test and the Vicker's test.

1.2.5. Small Punch Test (SPT)

In the case of bone samples, it is difficult to consider a big portion of the bone with the same thickness and architecture. In this and other instances, it can be necessary to use a

small sample in the testing as mentioned before. The Small Punch Test (SPT) allows us to test miniature samples with mixed forces of compression and shear.

The SPT was developed to characterize the samples in the power generation industry which relied on the accuracy of the mechanical test of a small representative sample (53). Other important applications of the SPT have been to characterize the microstructure of specimens such as UHMWPE[8] and PMMA[9], popular polymers in the biomedical industry, which have been used in joint replacement and anchoring applications (i.e. bone cements[10]) (53; 55). The SPT has additional benefits such as the capability of characterizing ductility in the plastic failure of samples (56).

1.3. Models for hyperosmolar solutions and hypertension

1.3.1. Animal models

An animal model is an animal used for the testing of pathological conditions and/or treatments that is aimed for human use or understanding. The United States has a strong culture of animal testing following the Food and Drug Administration (FDA) guidelines. Animal tests are conducted when there is a need to present preliminary test to the FDA, prior to human-subject experiments, and when testing on humans is unsafe or unethical (this last case is known as "the animal rule") (57).

[8] UHMWPE: Ultra-high-molecular-weight polyethylene which is usually abbreviated as UHMWPE is a common polymer in bone replacement applications because it is very resistant (54).
[9] PMMA: Poly (methyl methacrylate) is usually abbreviated as PMMA. It is a common polymer that due to it high stiffness (when compared to other polymers) is used for bone cement applications (53).
[10] Bone cements: Materials used to fix artificial joints (53).

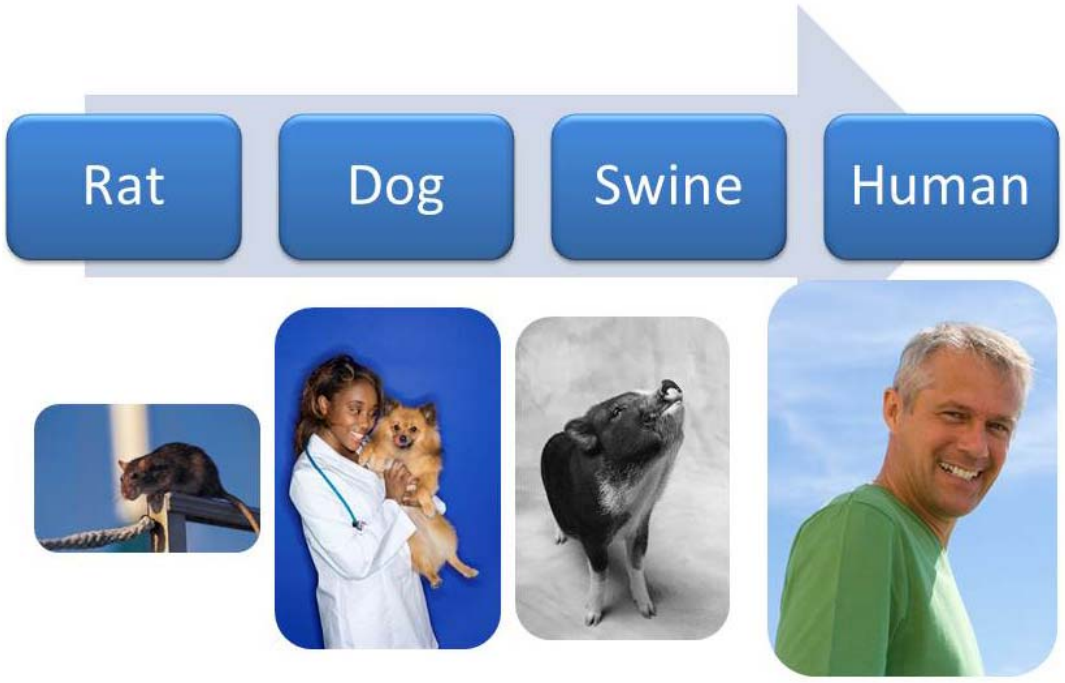

Figure 5 Animals and humans are used in cardiovascular research.

Efficaciously matching a disease or condition to an animal model can be a complicated task. Pigs have been successfully used in neuroscience research (21) with implementations in traumatic brain injury research (14); both of these developments justify a new use in intracranial hypertension research.

The pig has shown to be a good animal model in several other instances too which show the superiority of this animal model compared to other previously used in intracranial hypertension research (Figure 5). They have been used in bone research, since their bones remodel in similar patterns as humans (47), and in cardiovascular research because of similarities in the circulatory system anatomy, electrical activity of

the heart fibers, and other similarities (58). However, there have been few studies that characterize the bone of the head of the pig in detail. The only available studies that have researched swine skulls have focused in the mandible (25; 41; 59). Therefore the characterization of swine parietal and frontal bone areas during the present study can add detail to our existing knowledge of swine biology.

1.3.2. General mathematical models

Animal models are not the only way of studying pathological and physiological conditions. Computer models have become very powerful in recent years because they provide a cost effective way of exploring treatments and conditions prior to expensive animal models.

Because the use of salt solutions that are aimed at mitigating or reversing the effects of ICP could have severe consequences (e.g. they can cause increased intracranial pressure, alteration of heartbeat patterns, and the onset of adult respiratory distress syndrome (23; 24)), it is thus desirable to develop models that are aimed at the understanding of the interactions that hyperosmolar[11] solutions have on the elevated intracranial pressure patients.

Guyton was one of the pioneers who originally developed models for the study of the interaction of pressures in large mammals (60; 61). His model has been subsequently improved and revised, and thus provides a good foundation for this research. In this

[11] Hyperosmolar solutions or hypertonic solutions are solutions with a high solute content that are aimed at reducing the edema in the patient (1). Hyperosmolar NaCl solutions were used by Dr. Wolf to test his mathematical model (2).

model there are cross-references of results and analyses between the respective animal model (dog) and his empirical model. This model paved the way for further developments of mathematical models (60-62).

More than fifteen years later, Wolf developed a mathematical model that corroborated some of the results that were obtained by Guyton (63). This model did not account for the delicate ion balance between compartments, but included important elements such as the pressure, volume, and transport relationships present in the mammalian system (2; 63).

Gyenge took advantage of the vast information and equations from Wolf and Guyton and incorporated an analysis of the ionic balance of the systemic circulation and movement through four main areas, which he abstracted as mass transfer compartments. This last model involved twenty simultaneous differential equations solved with multiple auxiliary algebraic equations (23; 24) and systemic cardiovascular and tissue constants.

In order to maintain an adequate fluid balance, the body (with the exception of the brain) regulates itself mainly through the cardiovascular system, the hypothalamus and hormonal regulation (4). The mechanisms that it uses can be applied locally such as the constriction and dilation of the precapillary sphincters (4). The mechanisms can also impact the whole, as in kidney regulation, where these modulations aid in the regulation of the amount of fluid in the system (4).

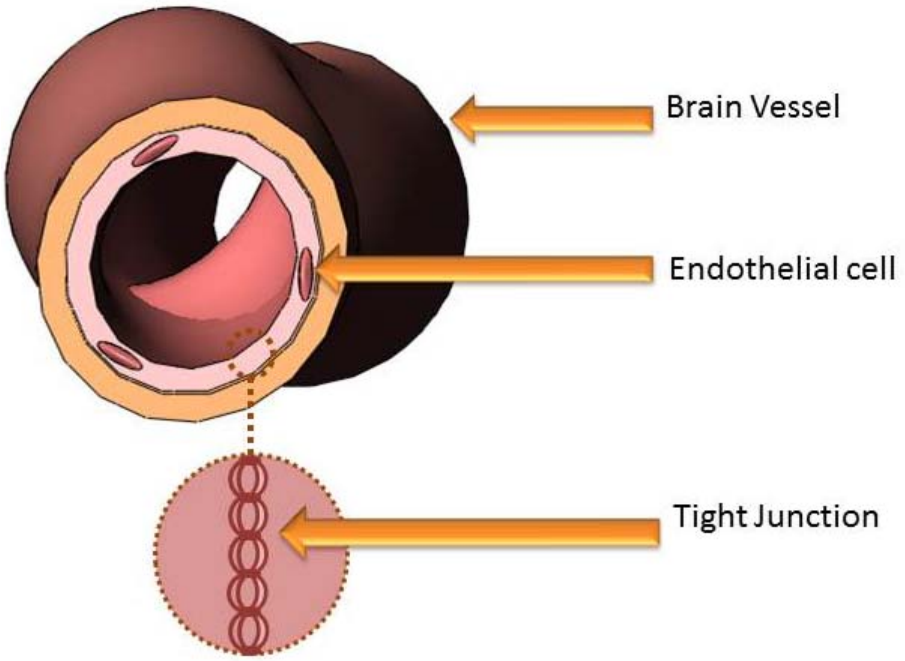

Figure 6 Tight junctions present in the brain.

The brain cannot be modeled following the same guidelines as the rest of the body, mainly because the circulation dynamics are different. The input from the arterial circulation into the brain gets regulated through tight junctions (Figure 6) that restrict the input and output of substances to the brain, which helps maintain a pathogen-free and toxin-free environment and homeostatic fluid balance (4). Additionally, the brain's biological homeostatic constants and parameters, such as hydraulic conductivity (64),

lack of lymphatic system (64), and lack of bodily fluid (the brain is surrounded by cerebrospinal fluid[12] instead of interstitial fluid) differ from the overall system.

Based on the general principles and formulas that were compiled into mathematical models by Guyton, Wolf, and Gyene we created an improved model that is relevant to the intracranial cavity. This model includes other principles and formulas not previously used in mathematical models of this nature before; therefore it is used to improve the understanding of this subsystem of the human circulation. A main input into the model is the possibility of including bone mechanics inputs that allow its reference to a real situation. The author recommends future testing *in-vivo* to make a final conclusion on the usage of this mathematical model.

[12] CSF: Cerebrospinal Fluid is a clear solution formed in the choroid plexus (region of the brain ventricles) that has protective properties (i.e. protective properties against a hit to the head and a tightly regulated environment).

CHAPTER II

MOTIVATIONS AND OBJECTIVES

As previously discussed traumatic brain injury (TBI) is a leading cause of death in the United States. The aftermath of TBI can be exacerbated because of the lack of information and faulty treatment modalities. Skull removal is practiced to relieve the pressure in the brain once the pressure reaches treacherous levels (≥20mmHg), but it is not a silver bullet because the pressure and volume relationships in the brain are mostly controlled by a blood brain barrier, which are a series of tight junctions surrounding the vessels. Hyperosmolar therapy[11] is administered in lower pressure levels, and although extensive research supports its more widespread use, the treatment has dangerous side effects.

Previous research suggests that the skull plays a role in establishing intracranial pressure and volume dynamics. This hypothesis is supported by thousands of clinical cases, as well as animal model experimental work, in which top portions of the skull were removed and its removal affected the pressure and volume related to intact skull measurements. Likewise, a softer and more malleable skull is hypothesized by the author to allow more volume fluctuations when compared to a sturdier skull.

The hypothesis ***is: salinous solutions have an impact on the mechanical properties of bone in vivo. The influences of osmotic agents could also change the mechanical properties of bone and influence the pressure and volume relationship of the intracranial cavity.***

In testing our hypothesis we designed the following specific aims which strive to find the pressure and volume relationships on a mathematically model of intracranial hypertensive patients. Such patients will have one of three hypothetical solutions, which are DPBS, hDPBS, and DI on their system. Each of these solutions has different osmotic coefficients and therefore generate variations in chemical potential in the blood. In order to test the model empirically we used bone soaked in different solutions as an input to the computer model.

1. Characterize the behavior of skull under different osmotic concentrations. There are two main experiments that aim at testing our hypothesis, which are:

(Note: These aims are practiced in the swine animal model because the test requires a high volume of samples and subjects.)

a. Development of a factorial experiment (see section 3.7.1) that compares the salt solution content and the cross head speed[7]. The solution chosen as control is DI water, and two high-salt solutions are also tested: PBS and hDPBS.

b. The bone extracted was cut in 2mm intervals. All of the 2mm, 4mm, 6mm, 8mm, 10mm, 12mm, and 14mm samples are extracted from individual skull cylinders (see section 3.7.1) which are statistically analyzed separately. This analysis is based on two saline solutions; hDPBS and PBS, in a factorial experiment. The aim of this experiment is to see if there is any difference between the solutions when analyzed with respect to the depth of the samples extracted.

2. Create an improved intracranial dynamics model which has the following unique properties:

a. Consideration of the skull influence on the pressure and volume modulation (inputs were obtained from motivation 1). This input is unique because the consideration of the skull influence has not been fully considered in similar models before.

b. Consideration of the pulsatile flow on the creation and movement of cerebrospinal fluid (CSF). Previous models consider the creation of CSF to be bulk flow or linear; however, more recent publications have shown the creation of CSF is sinusoidal in its nature due to the influence of the vessel pulsations.

c. Use of better methods of characterizing vessel behavior. Previously described models use formulas derived from curve fitting to characterize vessel behavior, but better methods are available for use. These methods rely on continuum mechanics models to predict the behavior of the vessel when pressurized. We use this method as an input to the model rather than traditional curve fitting methods, which can be less exact.

CHAPTER III

BONE MECHANICS

The relationship between hypertension and the skull rarely gets highlighted. It is important to understand how the bone interfaces with the intracranial cavity and how it reacts on the onset and treatment of hypertension, because this information will aid in the understanding of intracranial pressure (ICP).

3.1. The use of animals in scientific investigations

The use of animals for scientific investigations has been a tool available to researchers since antiquity. In the third century BC Erasistratus performed animal experimentation to study body humorous (64). In the nineteenth century the use of animals in experiments had become a standard practice (64). Today animal use plays a vital role in our society. Animal testing gets conducted prior to launching and/or testing cardiovascular devices in humans following the Food and Drug Administration (FDA) guidelines (65).

The FDA guidelines regulate the use of animals as models for pathological conditions, and these guidelines are stipulated under the Federal Regulation codes 21: CFR 314.600 and CFR 601.90. These codes describe what is known as the "Animal Rule" which is the testing of biological, pharmaceutical, and other products on animals when testing on human beings is unethical or not possible (57).

Animal studies are designed for their applicability to human situations (57). Matching animal models to their use can be very sophisticated, and proper and legal

handling of the animal needs to follow (65). Swine can be a successful animal model because of its cardiovascular (58), osseous (66), and neurological (21) similarities to humans (21).

In order to better understand the human hypertension conditions, mechanical characterization was implemented in skull samples embedded in osmotic solutions or water. The mechanical information that the test yielded needed to be used for elastic modulus[13] and peak stress calculations (comparison test for the solution effect on the mechanical properties). Therefore 10-20 samples were tested with the small punch test tool under 3 different strain rates and the information obtain was analyzed using ANOVA test.

3.2. Sample preparation

The sample preparation follows guidelines to ensure that the test conditions are as close as possible to the living situations. The bone is stored at -17°C and tested fresh once removed from storage. All samples are carefully machined and tested at room temperature (28). But as it can be interpreted from Table 1 further analysis is needed to understand this animal model because we can see that few areas of the swine have been investigated for their mechanical properties.

[13] Elastic modulus also called Young's modulus.

Table 1 Mechanical properties of swine bone.

Body Part	Peak Load (kg)	Peak Stress (MPa)	Modulus (MPa)
Mandible (59)	2.4±0.9	8.2±4.1	63.0±25.4
Metacarpal (59)	5.5±2.6	11.3±5.3	84.7±35.1
Zygomatic Arch (59)	16.4 ± 7.5	12.3 ± 4.6	91.7 ± 30.5
Vertebra (67)		15 ± 6	229 ± 138

The bone samples were tested with the load applied on the most exterior regions of the samples. This correlated to the skull under pressure from the inside, or as Figure 7 shows, +Z direction.

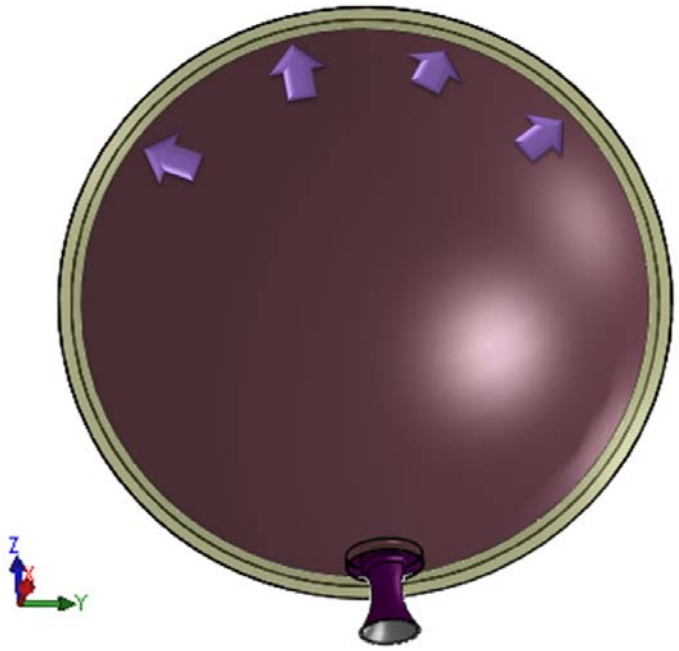

Figure 7 Pressure characteristics in intracranial hypertension. The samples obtained were taken from the frontal and pariental bone and tested in the +Z direction which will mimic the force depicted in this image.

Eight Sinclair Minipigs were used for the experiment. These animals were donated by the Texas A&M Institute for Preclinical Studies (TIPS). In the institute the animals were kept under laboratory conditions: diet and living conditions were kept stable. After sacrifice using barbiturates the animals were kept in a refrigerator inside a leak proof bag for 0-4 days. According to other authors, leak proof bag storage for less than 1 week does not affect the mechanical properties of the bone (28). In total, eight animals averaging 1 year old and 42 kg were used for the experiment. One female and

seven males were sacrificed. The use of these animals aided in the minimization of anisotropy because the animals had flat skulls in the areas extracted.

Figure 8 Sinclair Minipig with areas drilled.

In order to extract skull samples the swine was taken from the storage refrigerator and set up in a necropsy table. The quadrant of skin that covers the frontal bone and portions of the parietal bone was removed (from the end of the ears to the beginning of the eye area, Figure 8 and Figure 9). This area, which is flat in this swine species, ensures that the bone is even facilitating the drilling process and minimizing anisotropy. Once the patch was open for 1 cm, measurements were performed and traced

to draw a quadrant in the pig cranium. Intersections were used as guides for drilling areas; uneven areas were not drilled.

Figure 9 Swine drilling procedure on a 50 kg and 1 year of age swine.

During our preliminary studies several protocols were tested to ensure minimal damage to the cranium samples. Initially the tissues were cut and then drilled with a large-scale drilling machine. The force of the samples and sample preparation yielded uneven results; perhaps this was due to the damage of the samples in the machining process.

Figure 10 Tools for the bone extraction (drill, drill bits and Vernier).

The sample preparation for which the data yielded homogenous results was to use 3 mm diameter drill bits to drill on the cranium itself at ~2,500rpm (the tools used for the drilling procedure can be seen in Figure 10), which at this point of the investigation, was be approximated to break at ~9MPa (the peak stress of mandible the point at which fracture is produced in compression of most materials). Following its extraction the samples were immersed in the required solutions (please see section 3.3) and stored at -17°C for 2-3 weeks.

Although the aim of this study was to drill and extract a complete sample (whole contents of the swine skull), often the top portion (2-4mm), or the top and middle portion (2-8mm), will separate from the extraction of the sample and break inside of the pig. The skull has been described as a sandwich[14] structure of cortical bone, or heavier and sturdier bone in the exterior and cancellous bone (2-5mm), or lighter and softer bone, in the interior. These slight differences in structure and density probably made the composite separate. Therefore the areas that separated were assumed to be cortical or cortical and cancellous depending on the last layer of bone extracted. In Figure 11 we have an example of layers separating because of the difference in structure of the sample. In this instance the brown marrow was located in the middle of the sample; based on the color and location we can conclude that the exterior is cortical bone.

Following the procedures of other successful bone characterizations (29), the samples were allowed to acclimate to regular laboratory temperature for two (51) to three hours (28). Once the samples were acclimated, each rod (due to the extraction process the samples drilled had a rod shape of 3mm diameter and 2-14mm in length) was cut into 2mm intervals.

[14] Sandwich structures or sandwich panels are those composed of tougher exterior sheets that protect a softer and less dense interior (26).

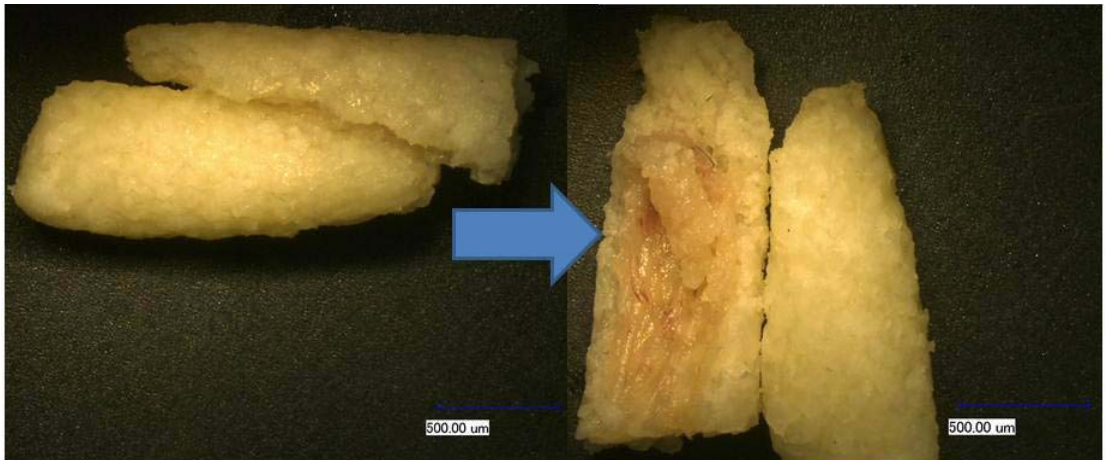

Figure 11 Cranium composition. Please note the separation of the layers due to the structure difference in the bone compositions.

The first 2mm of bone cut from each rod were analyzed separately for statistical significance following a factorial experiment that will be described in section 3.7.1. The next sample, which represented the interval 2-4mm from the cut rod, was also analyzed separately with other similar rod samples. This procedure was repeated seven times to span the 14mm, maximum length achieved in the samples obtained, Figure 12 exemplifies this procedure.

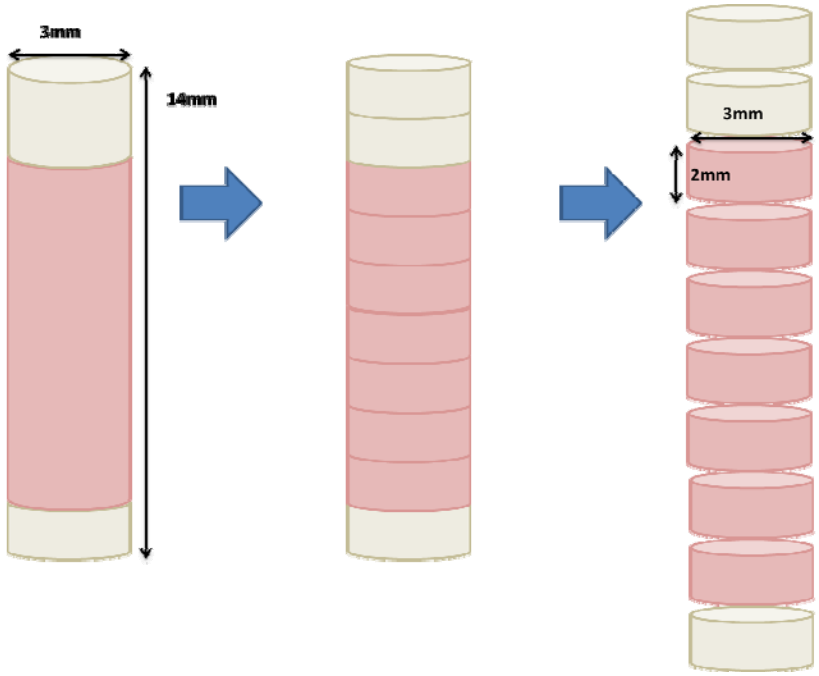

Figure 12 Sample preparation for the different millimeters obtained.

The samples were then cut using a thin blade with ~5N force to avoid breaking the small samples. In certain instances the cylinders extracted during the procedure were not exactly the size required. Certain samples were polished using a 320/P400 grit silicon carbide grinding paper to ensure the required size and surface roughness was 200±20 μm (Figure 13).

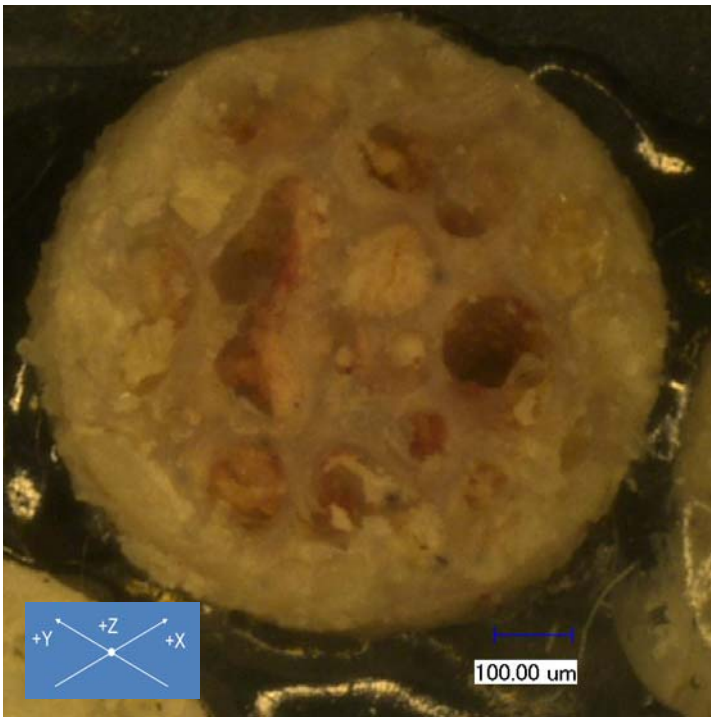

Figure 13 Samples extracted from the pig cranium. Please note the orientation of the osteon parallel to the +Z axis which ensured isotropy.

3.3. Osmolarity modification

The bone was stored for two to three weeks in three solutions: deionized water (DI), hyperosmolar diphosphate saline (hPBS), and diphosphate saline (PBS). The two saline solutions tested were comparable to those used by Dr. Gyenge in his osmotic experiments (24), 2000-24000mosmol/l (hyperosmolar saline) and 300mosmol/l isosmotic NaCl saline, and therefore provided a good point of cross reference with the bone test.

3.4. Bone mechanical characterization

The mechanical behavior of bone is less predictable than that of metals. Bone samples behave linearly-elastic at low strains and plastically at higher strains when they are wet. When dried the bone becomes more brittle (34). The small punch test can be applied to the mechanical characterization of ductile and brittle materials (55; 68).

The characterization of bone samples was attempted using the small punch test. The SPT tool is made of two encasings that have 3mm openings in the middle; the encasings are closed via four screws creating a cylinder that holds the sample in the center. Four legs are positioned next to the screws, and these legs can be pushed up and down to allow the encasing to remain until a load slowly lowers one of the encasings. The encasing has an opening in the middle that allows a 1mm ball bearing to be pushed by a piston-like tool. The system is laid over an Instron 4411 tensile and compression machine tester. A Solidworks drawing of the SPT can be seen in Figure 14.

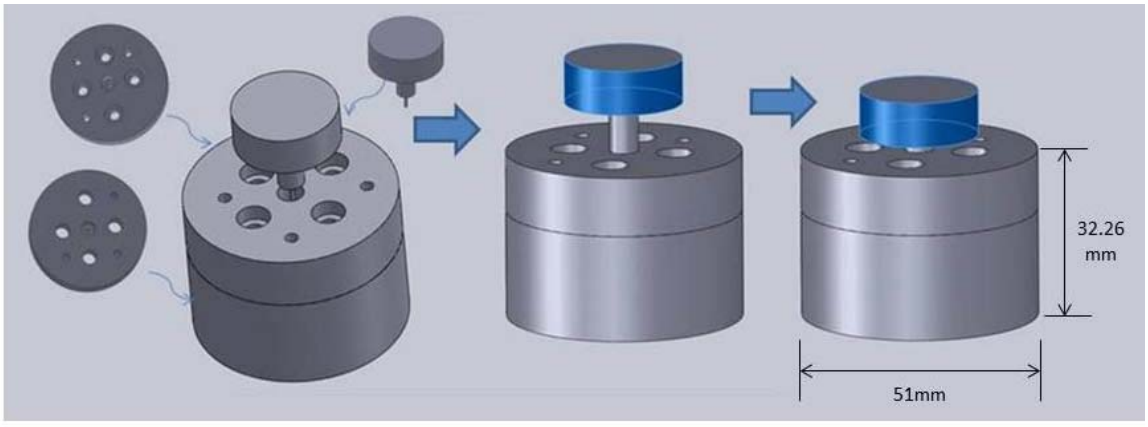

Figure 14 Small Punch Test procedure.

The Instron 4411 machine was used to produce the load in the experiment (Figure 15). There is a control panel with Texas Instruments Lab View software for control and data collection that allows the user to obtain the pertinent displacement information that is related to the prescribed load (Figure 15).

A force versus extension curve was then recorded in each trial. This curve corresponded to the information that the computer software extracted using the data acquisition system; this information is then displayed as a curve using LabView.

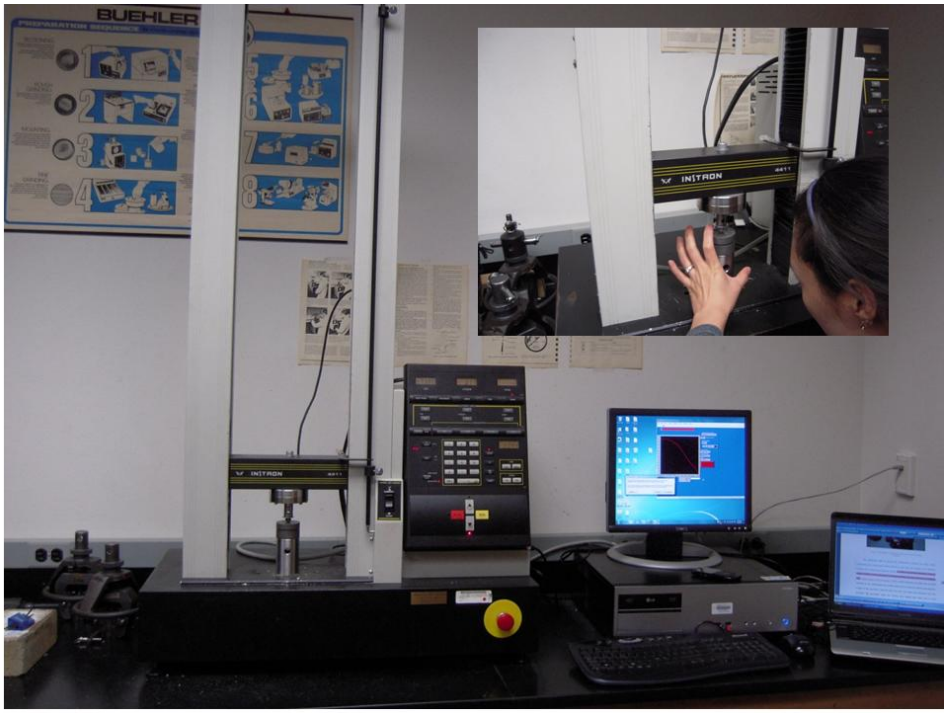

Figure 15 Representation of the Small Punch Test hardware and software.

The specimens under this testing were loaded until it was clear that the specimens reached a densification region. The time (minutes) that guaranteed us that the samples were densified were estimated using previous curves obtain while performing preliminary studies in swine samples. These curves allowed us to see how much testing time was necessary to obtain a Young's modulus [15] and peaks stress, which were important factors in the investigation.

3.5. Mechanical analysis

Cellular solids like bone can be characterized mechanically, even in cases in which they have seemingly haphazard behavior (26). Young's modulus can be calculated from the application of the Hertzian formula Table 2 (69). This formula had been applied in ceramic materials which were tested under compressive load with a variety of spherical tips (69).

Table 2 Hertzian formula for Young's modulus characterization (69).

Indentation (indenter and material) (69)	**Young's modulus (indenter and material) (69)**
$\delta = \left(\frac{3\mathrm{P}}{4R^{\frac{1}{2}}} \frac{1}{E^*} \right)^{\frac{2}{3}}$	$E^* = \frac{1-\nu_1^2}{E_1} \frac{1-\nu_2^2}{E_2}$

Where: P=load, R=radius, ν=Poisson's ratio, E= Young's modulus

[15] The Young's modulus (which is also called modulus of elasticity or elastic modulus) can be calculated from the slope of the stress strain curve in the initial linear elastic region of the graph.

3.6. Microscopy

Images of the specimens were taken before the mechanical testing to determine if any cracking had been caused due to handling of the material, and after the testing to verify the failure mode of the sample. Images were taken at 20x magnifications before testing, and at 20x and 100x magnifications after the testing. This allowed a broad perspective of the specimen. A Keyence VHX-600 digital microscope was used in conjunction with a Keyence microscope base and a Keyence VH-Z20 digital lens.

The analysis of the images before the mechanical test were done on random samples in order to verify visually the structural integrity of the samples and to possibly make a connection that could explain of statistical outliers. Only 20% of the samples were analyzed before the mechanical test was conducted and they were viewed quickly since there was the possibility of drying the samples, which could affect the mechanical properties (34).

Images obtained before testing were thus analyzed at 20x magnification only. Images taken after the bone was mechanically tested were analyzed to gain insight into the failure pattern of the bone. These images were taken at several magnifications (20x and 100x) and in both dry and wet conditions, which allowed a better perspective of the bone since the water can pose as a reflective agent. In these instances the shape of the bone cells and different components of the structure were observed. Also, an analysis of bone with different solutions was made.

3.7. Design of experiment and statistical analysis

In order to evaluate and draw adequate conclusions from our statistical data, we needed to find a point estimator[16] that could serve as a reliable predictor for the mean Young's modulus of the population. Common estimators for the population mean are: the sample mean, the sample median (the middle value of the sample data), and the average of the smallest and largest sample values (70). The sampling distribution determined which of the available estimators were applicable to our analysis. For instance, a sample mean estimator is applied when there is proof that the sample distribution is normal[17].

We used sample mean, trimmed mean, and median to test which point estimate was a reliable predictor for the population mean because: 1) the sample mean is one of most used population mean estimators; 2) the trimmed mean allowed us to reduce the variance in our statistical analysis; and 3) the median was a simple and widely used estimator.

3.7.1. Factorial experiments

We developed two factorial experiments to test the effect that three important factors had on the Young's modulus of the swine skull. In the first factorial experiment we compared the effect produced by osmotic agents and cross head speeds. In the second factorial experiment we compared the effect produced by osmotic agents and bone

[16] Point estimate: a statistics that serves as a guess (or estimator) of the true population parameter (i.e. the value that could exist if someone knew the behavior of all of the samples) (70).
[17] Normal distribution: when the distribution of the sample data follows a Gaussian function (70).

location. Table 3 shows the variables tested in the factorial test and the increments with which each variable was tested.

Table 3 The two factorial experiments developed in the current investigation.

Experiments	Factor 1 solution	Factor 2
1	DI	0.002 (mm/s)
	DPBS	0.004 (mm/s)
	hDPBS	0.02 (mm/s)
2	DPBS	Location : 2-14 mm (2 mm increments)

3.7.2. Statistical analysis

Due to the large variability in the samples it was necessary to compare different estimators for the sample mean. In the case of swine skull, a simple 5%-25% trimmed mean of the measurements ensures that the values behave mechanically and statistically the same. The results were trimmed discarding the lowest and highest values in all of the result sections prior to the analysis. These results were compared to the original mean and median of the sample. The trimmed mean samples were used in ANOVA statistical comparisons.

The analysis of variance (ANOVA) was tested for a null hypothesis that we had equal sample means (H_O: $\mu_1=\mu_2=\mu_3$=etc...) in the two comparisons; we tested the hypothesis taking into account a confidence interval of 95%.

3.8. Mechanical behavior of bone

Prior to the mechanical analysis of bone, the assumption that bone behaves like a cellular solid (Figure 16) was tested. Originally it was assumed that the behavior of bone resembled that of an Elastic-plastic material (Figure 17). However, preliminary mechanical tests showed that the mechanical behavior of bone was more complicated.

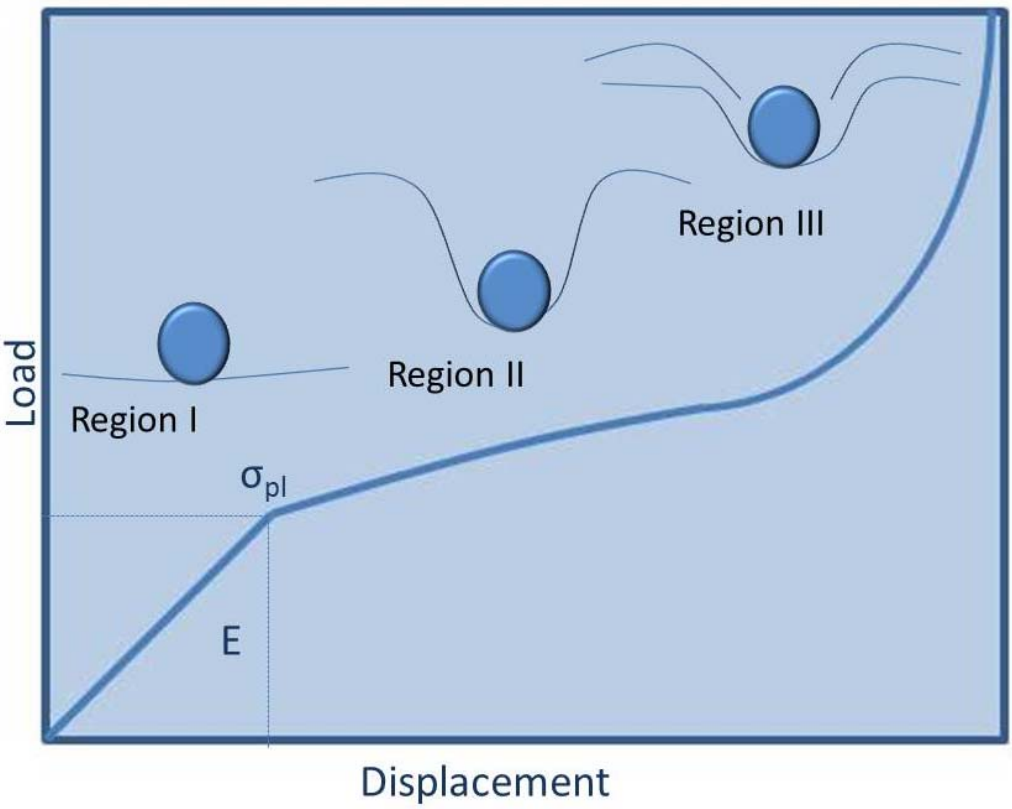

Figure 16 Mechanical behavior of cellular solids and sample behavior in an indenter test with high plasticity. In this figure we can see three clearly demarked regions: region I (linear elastic region), region (II) plateau region characterized by the failure of the material unit structure, and region III densification region characterized by a compaction of the material structures that give rise to an exponential growth of the material. The Young's modulus and peak stress σ_{pl} are also located in the Figure.

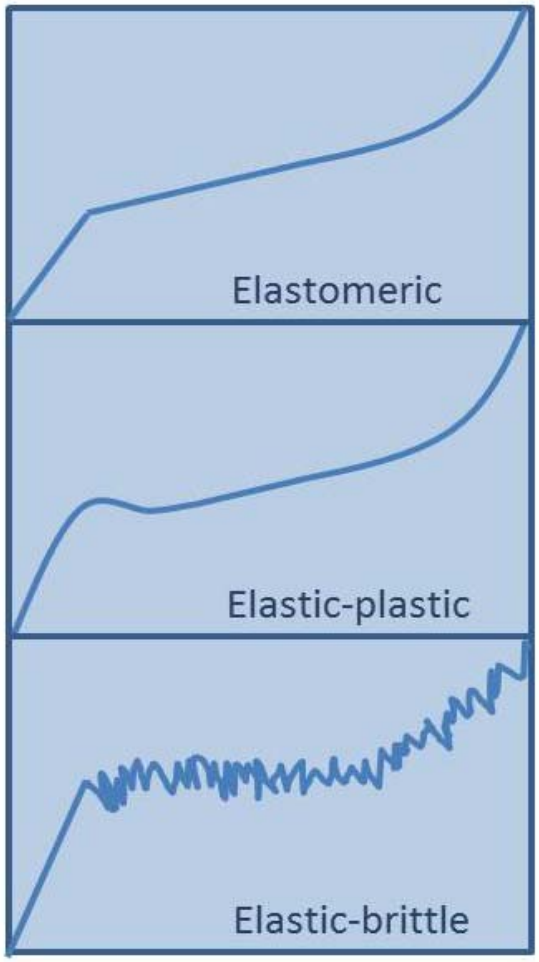

Figure 17 Compressive mechanical behavior of cellular solids with high elastic component (26).

In order to relate the mechanical behavior of bone to the change in the structure characteristics when the indenter is penetrating the sample we analyzed the microscopy of the samples. In this way we could see if the deformation was ductile, fragile, or elastic (buckling). We were able to see that the mechanical behavior of bone is more

complicated than was expected. The sample three-dimensional structure starts breaking when the indenter is pushed through the sample, as suggested in Figure 16. In this case the sample broke at a micro-structural level, which is evident by zooming into the force versus extension graphs (Figure 18) and by analyzing the microscopy of the sample (Figure 19). Because fracture characterizes elastic brittle behavior, this provided evidence to testify that the sample had fracture failure at least in the micro-scale.

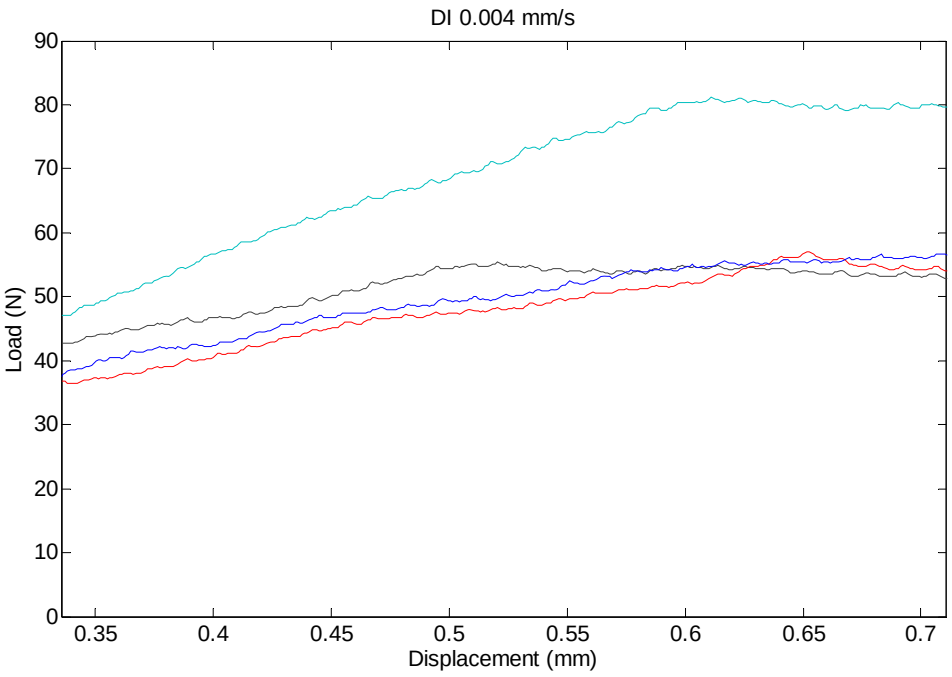

Figure 18 Elastic-brittle behavior of the material.

Figure 19 When bone is subjected to SPT the structures break as can be seen.

Additionally in the millimeter scale we can see that the sample had a clear linear elastic region; a plateau and a densification region (regions clearly identified in Figure 16). The linear elastic region gave into the plateau region in a sharp crest as opposed to a 'hump' (the two types of transitions are evident in Figure 20). We can conclude that therefore there is a mix of behaviors.

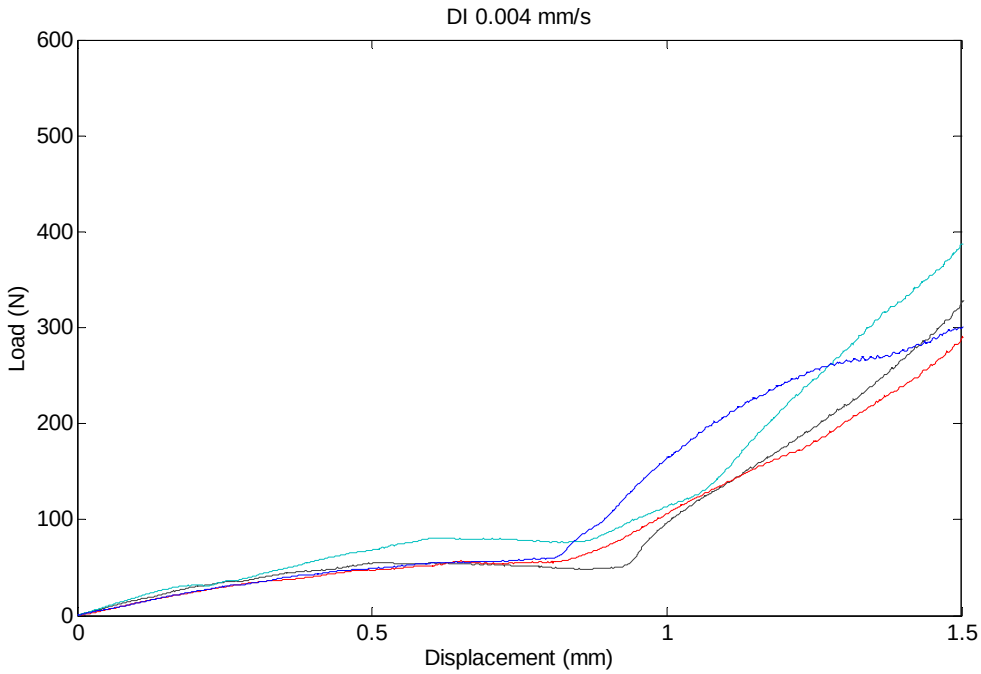

Figure 20 Elastomeric and elastic-plastic behavior of the material.

Additionally, we were able to see from the images that the indenter forces the sample until it breaks (Figure 19 and Figure 21), while the side regions of the material deform simultaneously. Because the material is an open cell solid, made of layers of bone in a three dimensional arrangement, breaking the sample from the top creates stacks of sample layers which allow the material to become denser when compressed.

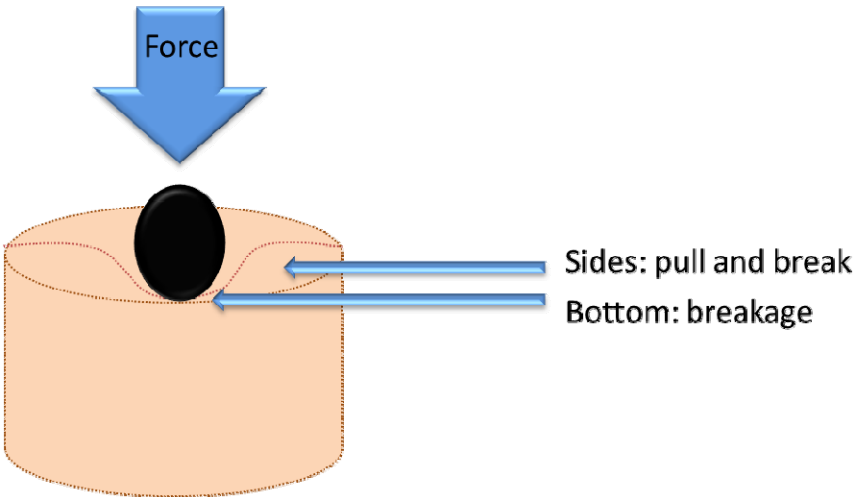

Figure 21 Application of the force in the SPT.

Finally, because our goal was to calculate the Young's modulus, and because the behavior is complicated, we analyzed the data in order to see the overall value of the peak stress. The peak stress functions as an input in the Hertzian contact stress formula (Table 2).

We were able to see that the peak stress value fluctuated around 0.2mm. In order to create an overall location for the peak stress for all of the samples we decided to set the value at 0.2 mm. From this pre-described peak stress we calculated the Young's modulus based on Table 2. We used the previous number because choosing a larger or smaller displacement location would mean choosing an outlier because most of the values were around 0.2 mm.

Figure 20 depicts the complicated behavior of bone, which is a mixture of the aforementioned elastomeric behaviors (Figure 17). The images also show that, when the

indenter pushes downward the material, the sidewise structures are pulled until they fracture; in other words, the bone fibers behave elastically until they yield plastically when pushed from the top and pulled from the bottom. The previously described force is characteristic of the force generated by a spherical indenter: a combination of compressive and shear force. Also, a similar reaction pattern of elastic deformation and plastic yield when the material was pulled from the bottom have been reported for other cellular solids with high plasticity (71).

3.9. Factors affecting the mechanical behavior of bone

In the mechanical characterizations of bone it was important to take into account how the material was affected by the input of the solution. In Figure 22 we can see that the mechanical behavior of the skull samples is slightly modified when treated with DPBS or hDPBS. In both instances we can see that the overall differences among the sample mean is minimal at 0.2 mm, the location of the peak stress. After the peak stress the linear elastic region ends and the plateau begins. Because the plateau and the linear elastic region are defined by their mechanical characteristics, the rate changes in the force versus extension curve graph signals the transition between one another (this rate changes are more visible in Figure 16 which was created to emphasize the difference in the three characteristic regions).

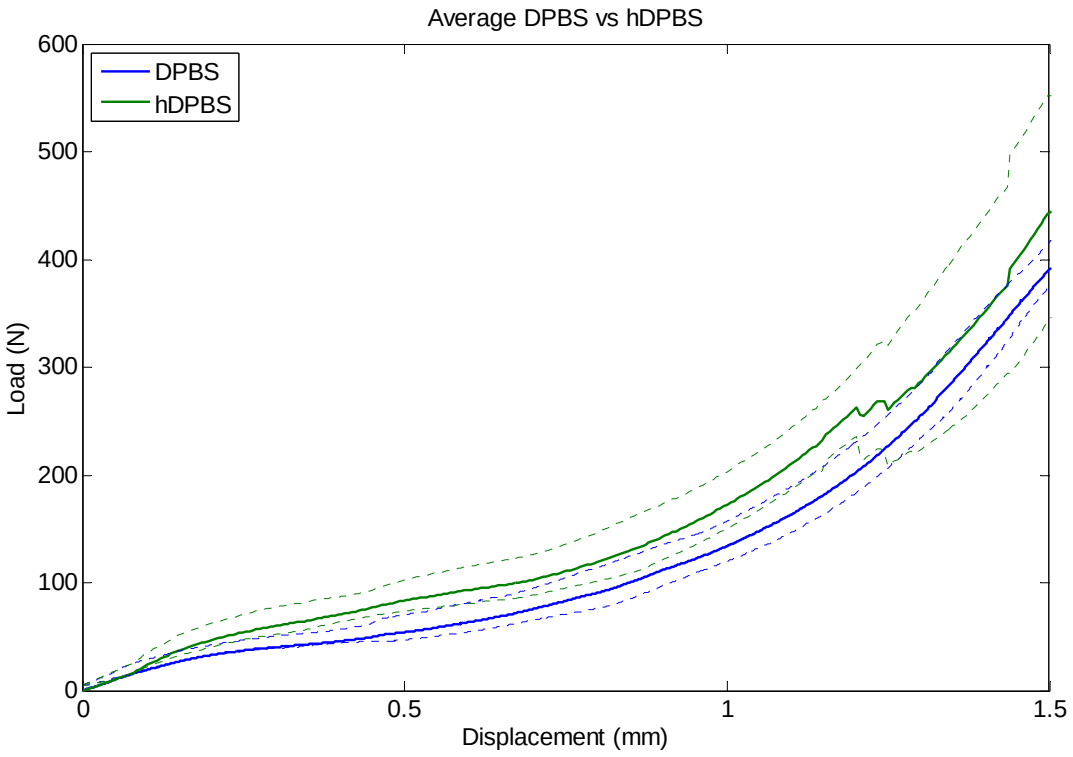

Figure 22 Mechanical behavior at different stages.

After the plateau the densification region takes precedence, as we can see near 0.75 mm in Figure 22. This region is the final region of the curve and is characterized by a sharp increase in the load the material can withstand per displacement (i.e. an exponential increase in the stress from a stress-strain curve). This region can continue until the sample is very compact; in our case we stopped the testing of the material when the sample was compressed to 1 mm in order to avoid damaging the SPT tool.

In these instances the statistical difference among the two samples with a negative hypothesis of same sample means at $\alpha=0.05$ is only $p=0.09$. While this is not a

statistically significant number, it is not extremely large and the value might suggest that if a higher concentration of sodium chloride was used in the experiment, it might have yielded a statistically significant difference. In Figure 23 we can see the mechanical behavior of the 2mm segments (segments of the bone analyzed separately). The skull structure is a biological sandwich structure[14] which is composed of a denser exterior made of whiter cortical bone and an interior formed of less dense cancellous bone (this structure has a soft pink hue due to the brown marrow) (Figure 12). Therefore we were able to see that the first 4 mm of the rod had a cortical bone morphology and color. The next 6 mm had a cancellous bone morphology and color. The last bone samples obtained were again whiter and denser; therefore they also appear to have cancellous bone characteristics.

The mechanical behavior of these different regions was the same as the previously describe behavior for cellular solids. There exists a linear elastic region, a plateau region with large deformation, and a densification region in which the samples become very compact. Therefore, in this region the sample withstands high loads, and the material behaves like a bulk material rather than a porous material.

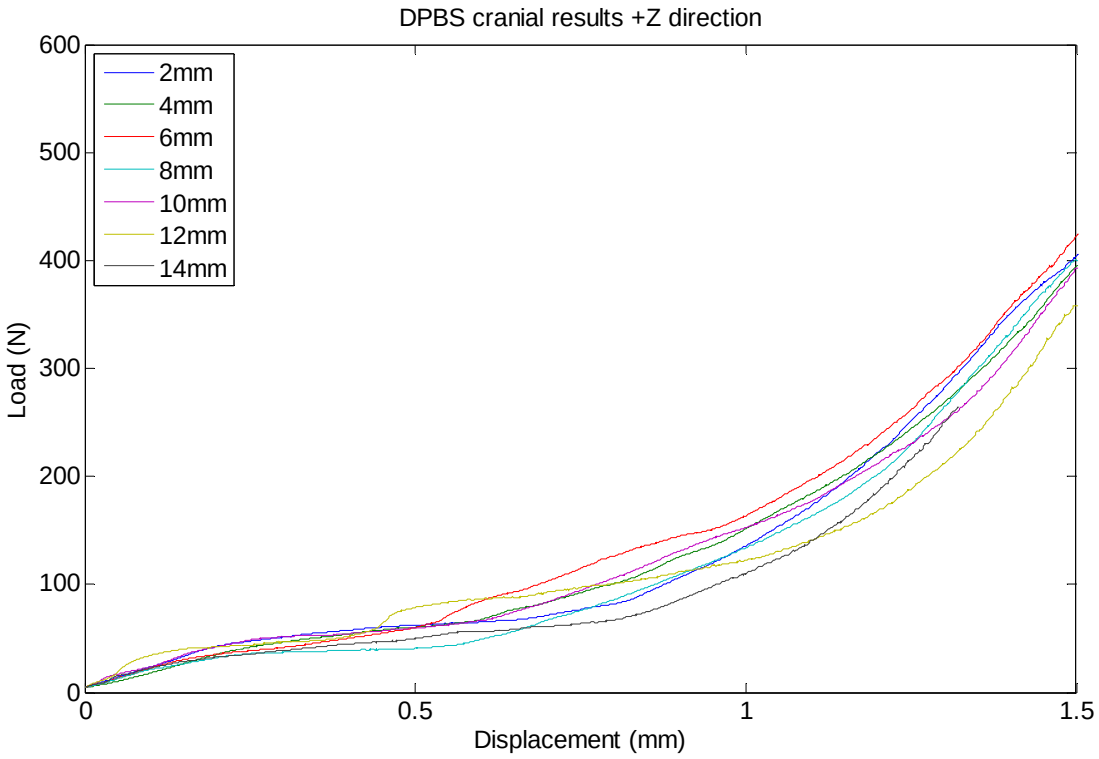

Figure 23 Behavior of the different regions of bone extracted.

The Hertz formula (Table 1) was used to analyze the linear elastic region. The inputs to this formula were the peak stress coordinates in the respective relevant units, the radius of the indenter and the Poisson's ratio for the indenter and the bone. Once this information was calculated the samples were statistically analyzed. The different locations of the rod that were analyzed did not yield statistical significances when analyzed for the difference in peaks stress. However, the factorial experiment that

compared the solutions used to the different cross head speeds used[7] yielded some statistically significant comparison pairs (Section 3.10).

3.10. Statistical results

It was difficult to analyze statistically the mechanical behavior of the samples because they had high variability. It was necessary to see the values of several statistical estimators for the population mean. In doing so we calculated the media, trimmed media, and the mean. These are reliable estimators for the population mean and therefore provided a good comparison for their usage in this application.

Figure 24 depicts Young's modulus calculated for the bone treated with DI solutions. In the case of DI, the trimmed mean could be a reliable estimator of the sample mean in all of the cross head tests done. This is because the two have seemingly comparable results with the trimmed mean having less variance. It can also be seen that the Young's modulus decreases with decreasing cross head. The mechanical behavior change between the samples that have 0.004 and 0.002(mm/s) cross head speeds is around the same as those of the samples with larger differences 0.004 and 0.02(mm/s). The difference in behavior was thought to be proportional to the change in cross head speed, but this test indicates no.

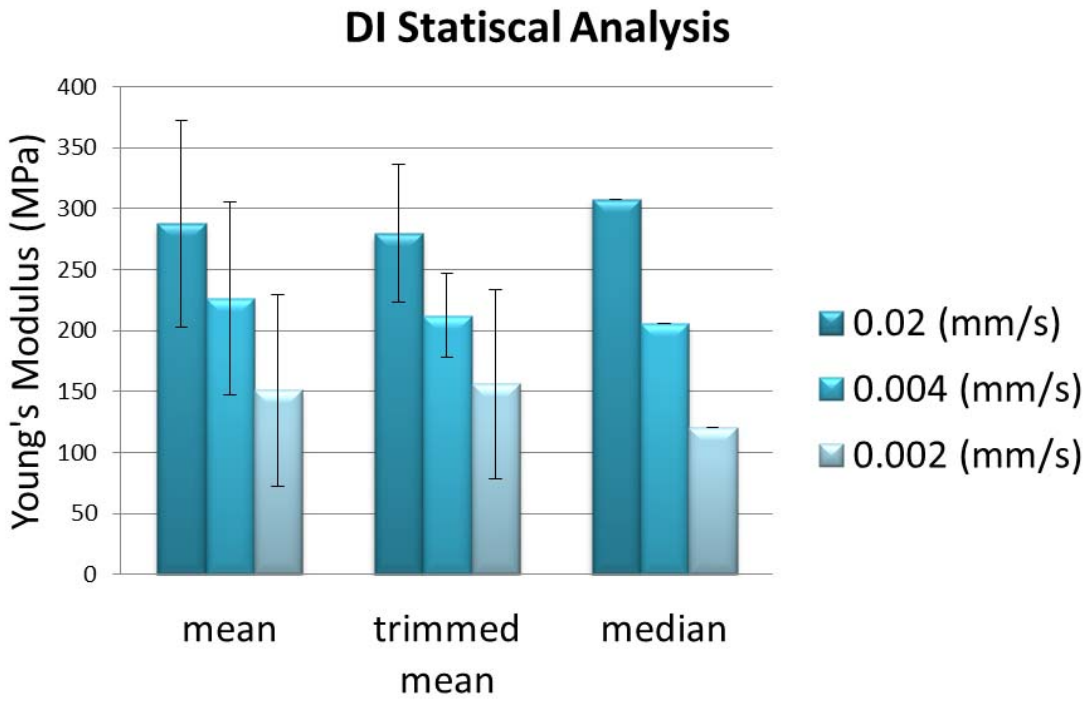

Figure 24 DI statistical analysis.

In the treatments of sodium chloride it was evident that, although the mean had slight variations between treatments, there were outliers. It is hypothesized that this is due to the variations in biological sample constitution and how the treatment affected the bone samples. However, that the variance is high, even when the samples are trimmed. It is believed that the solution concentrations are not exact in all of the bone samples because sometimes the solutions osmotically diffused differently through the samples, for example changes in temperature in the testing room could affect the mixing conditions of the samples and the osmotic coefficient of the samples.

Results reported by other authors that tested swine bone were faced with similar or higher values of variance (47; 67; 72). Because this variability was not found in other published studies on bovine bone it could be an indication that the swine bone has high variability (73; 74).

Because of the high variability a trimmed mean was preferred. The lower standard deviation allowed us to have an attempt at a statistical analysis since the analysis of variance (ANOVA) uses the variance of the samples for comparison. Using a trimmed mean is an approach that can be applied to biomedical samples which have large variability (75).

If the largest and smallest of the samples are trimmed, and there is evidence that by applying this consistently the samples yield statistically different results, then it will be suggestive that the samples may be different despite variability among replicates.

The statistical test yielded a p-value of less than 0.001, Ho of equal sample mean in the trimmed results of the Young's modulus samples vs. strain rate. The tests were robust with each containing 10-20 samples per test.

ANOVA comparison test also compares pairs for statistical difference when doing a comparison test for several combinations; this process is similar to a two sample t-test. From this second statistical test, the following combinations (Table 4) yielded a statistically significant p-value (less than 0.05). The values are presented with the mathematical difference between the means in order to provide insight into the great difference between the sample means in the Young's modulus results.

Table 4 Mean differences in statistically significant samples.

Solution Difference	Difference Between Means (Pa)
DI .02 (mm/s)-DI.002 (mm/s)	$1.05*10^8$
DI .004 (mm/s)-DI.002 (mm/s)	$8.97*10^7$
DI .02 (mm/s)-hDPBS.02 (mm/s)	$1.14*10^8$
DI .02 (mm/s)-hDPBS.002 (mm/s)	$1.08*10^8$
DI.02 (mm/s)- hDPBS .004 (mm/s)	$9.77*10^7$
DI .004 (mm/s)- hDPBS.02 (mm/s)	$9.95*10^7$
DI .004 (mm/s)-hDPBS.002 (mm/s)	$9.27*10^7$

3.11. Reasoning behind the change in the mechanical behavior

The fluid present in the bone pores can have an effect on the stiffness, work, density, and other calculations of the mechanical characteristics of the bone (34). Effort has to be taken to take into account the fluid present in bone, which is a part of its regular constitution if the bone is to be tested wet (26).

Calculations were made that compared the results obtained in the various solutions tested. Again, for this type of analysis the cellular theory was used. In this instance the theory takes into account the displacement of the solid, the fluid viscosity, the velocity of the fluid when it moves outside of the pores, strain rate, foam shape, and

temperature. The fluid trapped inside of the cell can have a larger contribution to the mechanical properties of the material when there is applied pressure (Figure 25). The contribution of the fluid to the strength of the material at the peak stress portion can be calculated using the formulas in Table 5.

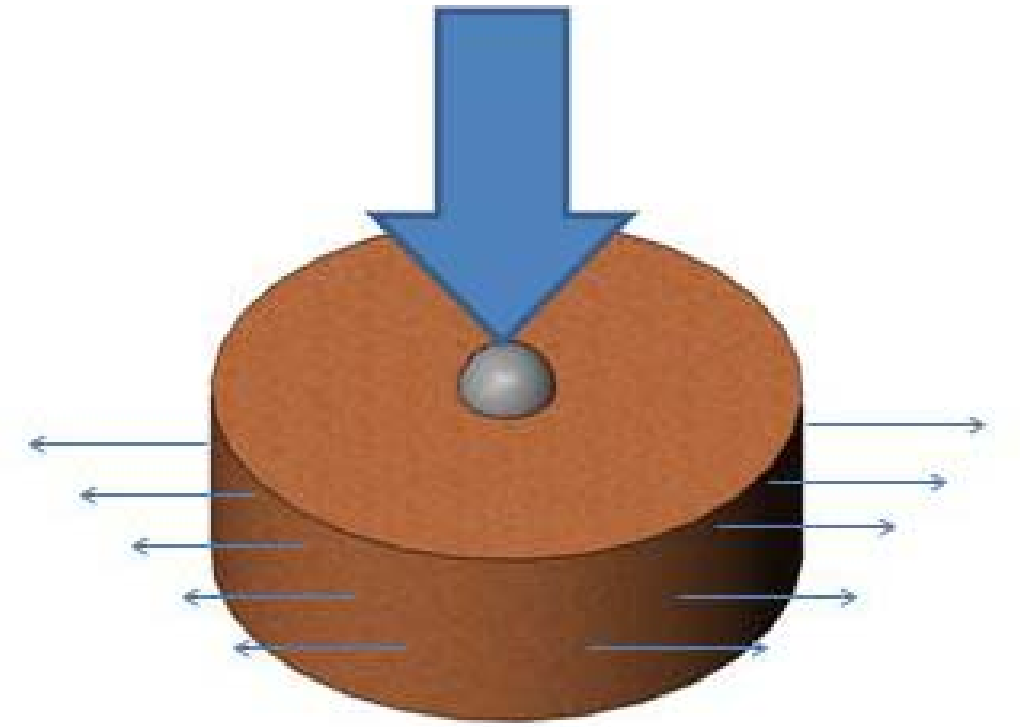

Figure 25 Cortical bone under indentation test. The fluid inside each of the cell structures has an impact in the overall behavior of the material.

Table 5 Equations used to solve for the mechanical stress of the bone.

Hardness solved for yield stress of foams (76)	**Strain at the initial of plateau after densification (76)**	**Contribution of fluid to the strength of the material (26)**
$H = \frac{P}{\pi a^2} = \sigma_y \left(1 - \frac{\left(\frac{h}{a}\right)^3}{\left(1+\left(\frac{h}{a}\right)^2\right)^{\frac{3}{2}}} \right)^{-1}$	$\varepsilon_m = \frac{d}{h} \approx \frac{a^2}{2Rh}$	$\sigma_g^* = \frac{C\mu\dot{\varepsilon}}{1-\varepsilon}\left(\frac{L}{l}\right)^2$

Where: σ_g^* =contribution of fluid to the strength, C =proportionality constant ≈1, μ =viscosity of the fluid, ε =strain, $\dot{\varepsilon}$ =strain rate, L =unit structure length considering a honeycomb, l =thickness of the trabeculae, a=the diameter of the indentation, R= the radius of the indenter, h= depth of the indentation and plastic zone under the indenter, P= force, σ_y =stress at a point.

In order to perform the analysis, a 0.1mm indentation ("h" Table 5) was considered to calculate the strain. This number was chosen because it correlated well with the total compression of the specimen in length (obtained by measuring the thickness of the specimen after testing). A simple mathematical relationship was then performed in this case, correlating the predicted strain, strain rate, and the length at the peak stress point. The values used the stress as an input and therefore the stress was calculated as well in Table 6.

Table 6 Calculated stress of swine bone used to compare the fluid contribution.

	Cross Head (mm/s)	DI		NS		HYP	
Value		μ	STD	μ	STD	μ	STD
σ (MPa)	0.02	53	11	32	15	30	18
	0.004	41	12	36	10	31	21
	0.002	2.7	12	39	13	31	22

The result of this difference is depicted in (Table 7). Here we can see that the difference is high because this represents the value in just one point. The summation of all of the information can yield quite a difference considering that the value can be compared to the 1mm diameter indenter.

Table 7 Stress contributions solutions for the fluid contributions to mechanical properties of bone.

	Solution		
Cross Head (mm/s)	DI (Pa)	DPBS (Pa)	hDPBS (Pa)
0.02	$2.16*10^{-5}$	$2.28*10^{-5}$	$9.15*10^{-5}$
0.004	$4.5*10^{-5}$	$4.75*10^{-5}$	$14.0*10^{-5}$
0.002	$2.25*10^{-5}$	$2.37*10^{-5}$	$9.51*10^{-5}$

CHAPTER IV

MATHEMATICAL MODELING OF INTRACRANIAL HYPERTENSION

TBI is one of the leading causes of death in developing countries (17). It creates primary and secondary. The initial tissue damage that happens at the moment of the impact is the primary pathway. It can cause the creation of pores in the lipid bilayer, which in turn can create a misbalance in the concentration of ions in the cell plasma (e.g. potassium, intracellular sodium, chloride and calcium) (14). These non-homeostatic ion levels can then cause grave consequences such as apoptosis and edema (14). Figure 26 highlights three pathways that cause cell injury and death as a result of calcium ion mismatch in the cell plasma levels (14).

The portions of the responses that happen as a result of the primary injury, but occur at a later time, are called secondary injury responses (1; 17). These negative responses can further endanger the health of the patient. For example the inflammatory response can be so severe that the blood supply of the patient is disrupted (77). Table 7 states some of the symptoms, consequences, and treatments of the overall injury caused by TBI. This table was organized by the most affected organ systems.

From Table 8, one of the secondary injury responses that is closely monitored for its risk, is high blood pressure in the intracranial cavity (ICP) caused by the inflammation of the injured areas. High blood pressure can further damage the tissue and it has been implicated in the decrease of blood supply to the tissue (78). Therefore is no

surprise that patients with TBI who experience intracranial hypertension generally receive poor prognoses (16; 17; 79).

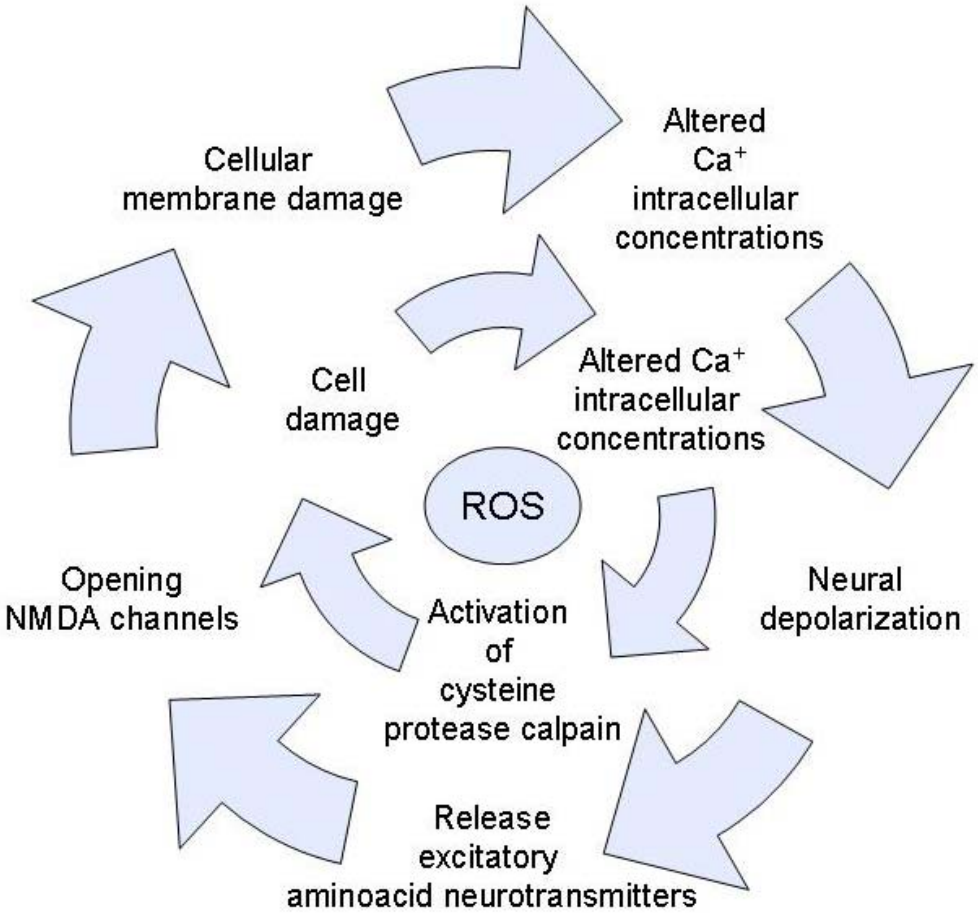

Figure 26 Cell death/injury pathways caused by calcium mismatch in the cell plasma.

Table 8 Table depicting: the symptoms of TBI, the beneficial effects of the therapy, the nocive effects of the therapy and the overall outcome.

Sys.	TBI symptoms	Beneficial HTS effect	Nocive HTS effect	Overall Outcome
CVS	Calcium damage, ischemia, edema, high ICP (14).	Increase heart contraction, increase in cardiac output by a reduction in vascular resistance (1; 80), plasma expansion (1; 81).	Hemodilution (82) which can cause hypoxia, acidosis, organ failure, etc (1), hypernatremia, hyperosmolarity (24; 83), among other conditions.	Overall good recovery (84) outcomes from acute hematoma are the following : epidural 75%, subdral 23%, intracerebral mass lesion 12%, diffuse brain injury 40% (85).
Endocrine	Pituitary can get affected leading to hypopituitarism (86).	Increase hormones and endothelins, e.g. cortisol (1; 80).	Please see immune and CVS cells the whole system is related.	Following published guidelines (84) the outcomes to Anterior Pituitary dysfunction in TBI are: good recovery 55.9%, moderate disability 32.3%, severe disability 11.8% (87).
Immune	Secondary injury can activate resident immunocompetent cells, secreation of intrathecal cytokines and (88).	Increase in secretion of prostanglandins (80) and decline of the adherence of leukocytes (1; 89).	There is evidence to the modulation of the brain's inflammation responses by the immune system (90). An adverse response can be understood as a decrease of this response to a point that is not beneficial by HTS, but this information has not been found reported.	
Nervous	Auxonal injury due to a disruption of the proteins present in the cytoskeleton (14).	Restoration of osmotic balance (Figure 26) (1; 89).	Adverse responses to the CVS are occurring in the brain; both of these systems are affected (see CVS cells). Demyelination can occur (91).	Overall good recovery (84) outcomes from positive key neurological responses are the following: motor 61%, oculocephalic 66%, pupilary light 85%, overall good/moderate recovery 64%(85).

.

4.1. Treatment

The treatments applied for TBI vary, but there are some guidelines that are followed: the doctors monitor the intracranial pressure if the patient is neurologically compromised (GCS score[18] less than 9) (92). After the dangerous pressure of 20 mmHg is reached, the doctor has to ensure that the patient has no obstruction to flow and no hematomas (the patient is drained) (77; 92); at this point a craniectomy and osmotherapy are recommended (77). Additional therapies are practiced as directed by Figure 27.

The administration of osmotic agents for the treatment of TBI has been studied extensively (1; 82; 93-96). These studies include animal, mathematical, and analytical models (60). The mathematical models used have employed the most recent information available to create the necessary codes. For example, Wolf's model (63) uses a fitted equation from the work produce by Guyton to describe the behavior of the interstitial fluid pressure (60).

In our case we attempted to update the current models to include new constants, the mechanical vessel behavior (based on continuum models) and the mechanical behavior of bone, which have an impact on the overall intracranial hypertension behavior. Studies have shown modifications in the morphology of the skull with ICP changes (7), and the lack of cranium has been implicated in the modification of pressure-volume relationships present in the head (97; 98). Therefore, we used the current models

[18] GCS score: GCS score is a set of characterizations that are assigned to neurological status in cases of TBI and other head injuries (13).

and formulas to test the role the cranium has in the intracranial pressure-volume modulations.

Additionally, we based the arterial compartment compliance on current constitutive relationships that relate changes in radius to changes in pressure (52) and we based the formation of the movement of cerebrospinal fluid on pulsating (Womersley flow) calculations.

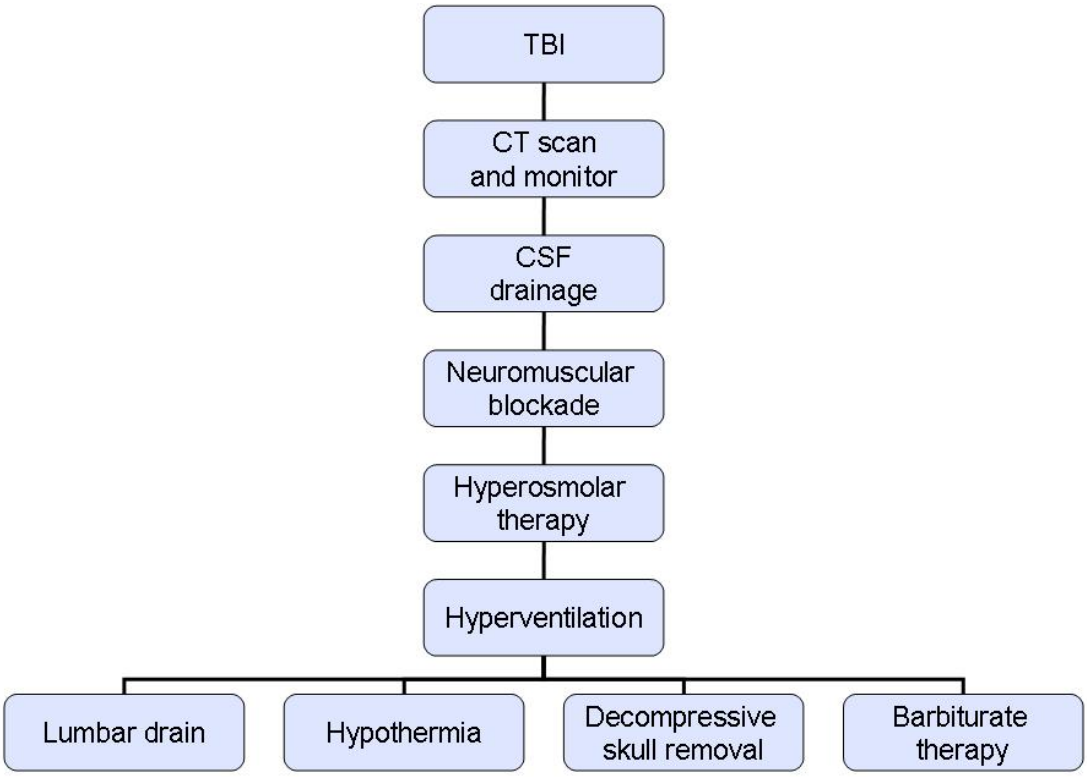

Figure 27 Treatment modalities for TBI.

4.2. Calculations for the determination of factors in the intracranial hypertensive model

4.2.1. Pulsatile calculations for the determination of CSF

For years it was assumed that the flow of water and substances through the brain and into the brain ventricles was through bulk flow (99-102). More recent investigations suggest that this movement occurs by the propulsion that the vascular system pressure waves cause when they travel through the brain (103), which is reliant on the vessel elastic properties (104). Pulsatile flow calculations allow this movement to be analyzed.

Table 9 Fluid flow formulas used for the analysis [103].

Meaning	Equation (105)
Flow rate Poiseuille	$Q = \frac{\partial p}{\partial z}\frac{\Pi a^4}{8\mu}$
Velocity rate Poiseuille	$Vz = -\frac{\partial p}{\partial z}\frac{(a^2 - r^2)}{4\mu}$
Velocity rate Womersley	$Vz = \frac{A}{i\rho\omega}(1 - \frac{J_0(i^{3/2}\alpha\ r/a)}{J_0(i^{3/2}\alpha)})e^{i\omega t}$
Flow rate Womersley	$Q = \frac{\pi R^2 A e^{iwt}}{i\omega\rho}\left[1 - \frac{2J_1(i^{3/2}\alpha)}{i^{\frac{3}{2}}\alpha J_0(i^{3/2}\alpha)}\right]$

One mathematical description that takes into account periodic pressure gradients is Womersley Flow. Womersley studied the pulsatile blood flow through arteries by using classical principles such as the continuity equation and pressure. Unsteady flow is added to the steady solutions to determine the whole nature of the flow therefore there is a need to provide a waveform input to solve for the other variable (in Figure 28 we can see how the basilar arterial waveform was fitted using Fourier transform principles) (106; 107). Therefore, the unsteady and steady flow through tubular vessels was then added to the code in order to generate fluid flow patterns through the brain vessels and into the ventricles (Table 9).

Summarizing, when solved for the boundary conditions at the vessel wall, Poiseuille flow describes the steady and laminar flow through straight tubes. This equation is expressed in spherical coordinates and has inputs of pressure and viscosity. Womersley flow is used to describe the non-linear pulsatile flow through the vessel.

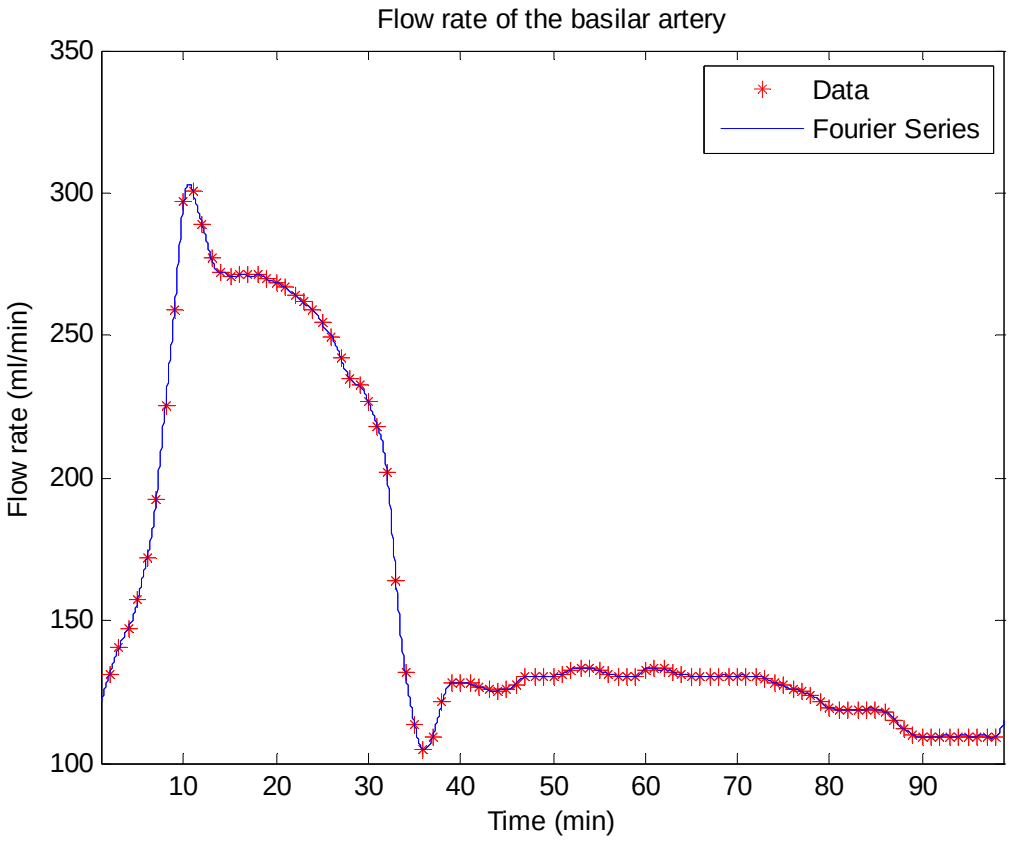

Figure 28 Basilar flow rate waveform with a Fourier transform was applied to it following equation 15 (in the table).

4.2.2. Constitutive framework of vascular compliance

The description of vessel compliance in mathematical models has usually been obtained through empirical observations (63), curve fitting (60; 63), and basic computer simulations (108). Constitutive models that describe the behavior of vessels have been developed by Dr. Fung, but have not been applied to this instance (52). Descriptions of the common carotid and modifications of the radius, and constants of these descriptions,

were used for the compliance input in the model for the two compartments instead of relying on curve fitting of previous animal studies.

Published analysis was recreated using the following equations of W, Q, Cauchy stress, and green strain in spherical coordinates. The formulas used were coded to solve for the pressure inside of the vessel and the relationship to the radius. This information was used to solve for the compliance of the vessel per radius, which correlates with time since there are fluid inputs. The formulas in Table 10 and constants present in Table 11 were added to the general code.

Table 10 Equations to determine the hoop stress of the vessel.

Meaning	Equation (105)
Strain energy function	$Q = \frac{1}{2}c_1 E_{\theta\theta}^2 + \frac{1}{2}c_2 E_{ZZ}^2 + c_3 E_{ZZ} E_{\theta\theta}$ $W = -c\ln(1-Q)$
Cauchy Stress	$t_{11} = \left(\frac{c}{1-Q}\right)\lambda_\theta^2 (c_1 E_{\theta\theta} + c_1 E_{ZZ})$
Cauchy Stress	$t_{22} = \left(\frac{c}{1-Q}\right)\lambda_Z^2 (c_2 E_{ZZ} + c_3 E_{\theta\theta})$
Green Strain	$E_{\theta\theta} = \frac{1}{2}\left[\lambda_\theta^2 - 1\right]$
Green Strain	$E_{ZZ} = \frac{1}{2}\left[\lambda_Z^2 - 1\right]$
Extension in the circumferential direction	$\lambda_\theta = \frac{Di^p - Do^p}{di - do}$

Table 11 Constants used for the analysis.

Meaning	Constant	Human Specific
Constant	c1 (KPa)	0.40206
Constant	c2 (KPa)	0.3847
Constant	c3 (KPa)	0.0225
Undeformed external diameter	do (mm)	2.411
Undeformed internal diameter	Di	3.541
Deformed external diameter	D0	4.852
Deformed internal diameter	Di	4.431
Extension in z direction	λ_z	1.72

4.3. Compartmentalization model

We designed a theoretical compartmentalized model during this investigation. The model is based on 7 main compartments as can be inferred from the drawing (Figure 29): a brain arterial compartment, vascular compartment, venous compartment, brain compartment, skull compartment and ventricle compartment. This model was solved analytically with the equations presented in Table 12 using MATLAB®.

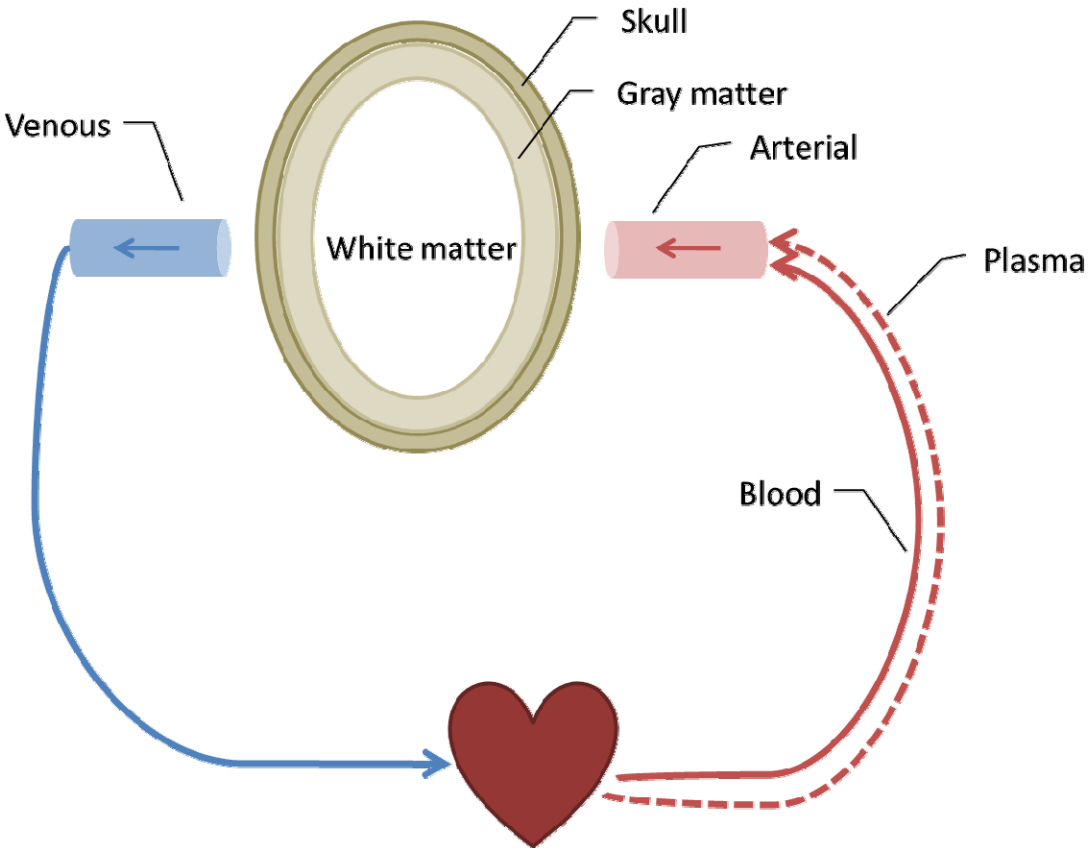

Figure 29 Theoretical compartmentalized model.

Due to the constraints in MATLAB®, solving for a direct non-symbolic differential-algebraic initial value problem simultaneously was not possible (unlike Maple or other computer languages); therefore the code was run in pieces. First the variables and values (present in Table 11, Table 13 and the cited papers) were compiled and run in a MATLAB® symbolic subroutine that enabled the creation of large solutions for unknown differential equations.

These equations were then solved simultaneously using a function for simultaneous differential initial value problems and then retrieved, compiled, and graphed. The values were compared to other literature featuring swine traumatic injury study.

Table 12 Code related equations.

Meaning		Equation and Author
Main volume relationship brain	1	$V_{Blood}+V_{CSF}+V_{Brain}$ (109)
Capillary starling relationship in the (protein and salt)	2	$J_{cap}=L_{cap}\left[\left\{P_{plasma}-P_{tissue}\right\}-\sigma_{protein}\left\{\pi_{protein,plasma}-\pi_{protein,tissue}\right\}-\sigma_{salt}\left\{\pi_{salt,plasma}-\pi_{salt,tissue}\right\}\right]$ (109)
Solute pressure	3	$\pi_s = RT \cdot S$ (63)
Protein pressure	4	$\pi_c = 2.1 \cdot C + 0.16 \cdot C^2 + .009 \cdot C^3$ (63)
Volume relationship compartments • **capillary** • **red cell**	5	$\frac{dV(t)}{dt} = Iw(t) + \sum_j J_{V_j}(t)$ (24; 63)
Total volume	6	$V_t = V_c(t) - \sum_{k=1}^{5} V_j(t) + \int_0^T I_w(t)dt$ (63)
Volume relationship in the capillary	7	$\frac{dV_{Vi}}{dt} = C_{Vi}\left(\frac{dP_v}{dt} - \frac{dP_{ic}}{dt}\right)$ (108)

Table 12 Continued.

Meaning		Equation and Author
Volume relationship in the capillary II	8	$\frac{dV_{Vi}}{dt} = \frac{P_c - P_v}{R_{pv}} - \frac{P_v - P_{vs}}{R_{vs}}$ (108)
Blood brain barrier threshold	9	$\left(\pi_{salt,plasma} - \pi_{salt,tissue}\right) + \left(\pi_{oncotic,plasma} - \pi_{oncotic,tissue}\right) \rangle (P_{plasma} - P_{tissue})$ (109)
Intracranial storage capacity	10	$C_{ic} \cdot \frac{dP_{ic}}{dt} = \frac{dV_{pa}}{dt} + \frac{dV_{Vi}}{dt} + q_f - q_0$ (108)
Pressure plasma	11	$Pi(t) = Pi^0 + \frac{[Vi(t) - Vi^0]}{\gamma_i W}$ (23; 63)
Pressure capillary	12	$P_{cap} = P_{cap,nom} + P_{cap,com} \cdot (V_{pl}(t) - V_{pl}{}^0)$ (23; 63)
Bone and Young's modulus relationship	13	$\frac{\Delta P_N}{\Delta P_v} = \frac{\left(\frac{E_b}{3}\right)\left(\frac{1}{R_N^3 - R_S^3}\right) + \frac{E_S t_s}{R_S^4}}{\left(\frac{E_b}{3}\right)\left(\frac{1}{R_v^3 - R_S^3}\right) + \frac{E_S t_s}{R_S^4}}$ (110)
Hematocrit	14	$Hct = \frac{V_{RBC}}{(V_{RBC} + V_{PL})} \times 100\%$ (23)
Fourier modeling of transient data	15	$y = a_0 + a_n \cdot \cos\left(\frac{2 \cdot pi \cdot n}{99}\right) ... + b_n \cdot \sin\left(\frac{2 \cdot pi \cdot n}{99}\right) ... + a_{49} \cdot \cos\left(\frac{2 \cdot pi \cdot 49}{99}\right)$
Womersley Model for the determination of CSF flow	16	Please see previous descriptions
Fung's Strain constitutive equation	17	Please see previous descriptions

Table 13 Main constants used for the mathematical model (111).

Constant	Regular Brain	Edema
Capillary Flow J^{cap}	$1.1*10^{-3}$	$11*10^{-3}$
Capillary Conductivity L^{cap}	$1.5*10^{-3}$	$1.5*10^{-3}$
Osmotic reflection coefficient of the tissue σ_{oncoic}	1	0.93
Osmotic reflection coefficient of the salt σ_{salt}	1	0
Hydrostatic pressure plasma $\Pi_{salt,plasma}$	5100	5100
Hydrostatic pressure tissue $\Pi_{salt,oncoic}$	25	25
Osmotic reflection coefficient of the salt σ_{salt}	1	0

4.4. CSF movement and creation

The pressure, volume and ion dynamics of the intracranial cavity are for the most part modulated by the vessel's integrity. Intracranial vessels are bounded by tight junctions that enforce a strictly regulated environment inside the cavity. However, the creation and movement of the CSF through the system is regulated through pulsations. These pulsations create pressure waves that can be traced to the movement of fluid in and out of the ventricles and into the venous system (Figure 30).

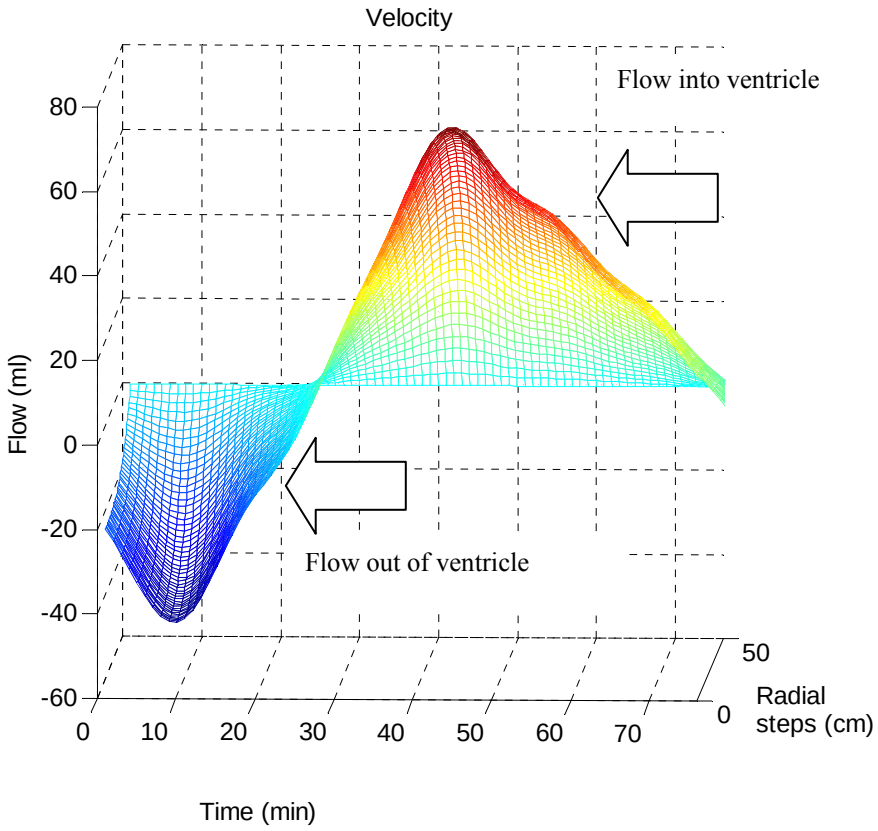

Figure 30 Velocity flow rate (ml/cm/s) generated by Womersley flow. These results show how the waveform in fact can create the inflow and outflow patterns that have discussed earlier and which can be corroborated with other studies.

4.5. Volume in different compartments

In Figure 31 we can see the behavior of a vessel when it is being pressurized. As the pressure increases the vessel diameter increases to a point in which the increase diminishes. This time-wise compliance relationship has not been used as a compliance input in the past. This information was coupled with the information obtained from the other equations in order to obtain pressure and volume values for the brain cavity.

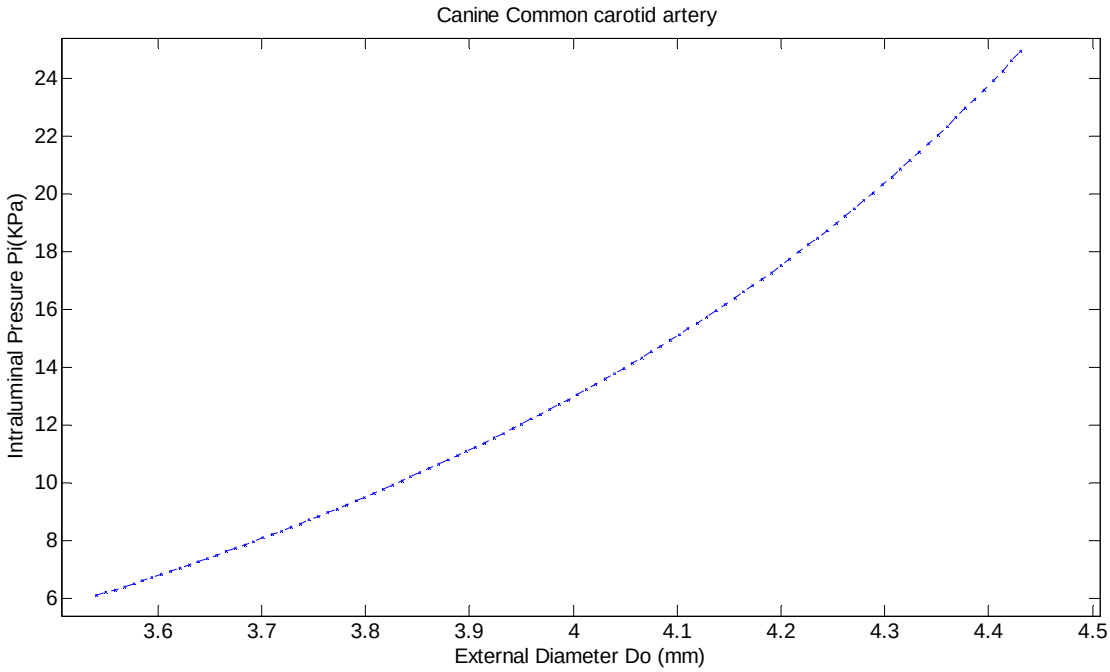

Figure 31 Pressure vs. diameter for the femoral artery generated by published constants. The information was in turn related to the compliance of vessel.

The following results represent information obtained from the formulas and simulations described in the previous sections of this chapter. These values were compared to the values obtain from the authors of the formulas (2; 23; 24; 63).

Figure 32 represents the interstitial volume change in the systemic circulation and its change when there is salt in the system. We can see that there is a negative correspondence in the two values, which correlates to the shifts in the volume in the compartments. This mechanism will be affected by the salt concentration in the plasma and similarly in the brain.

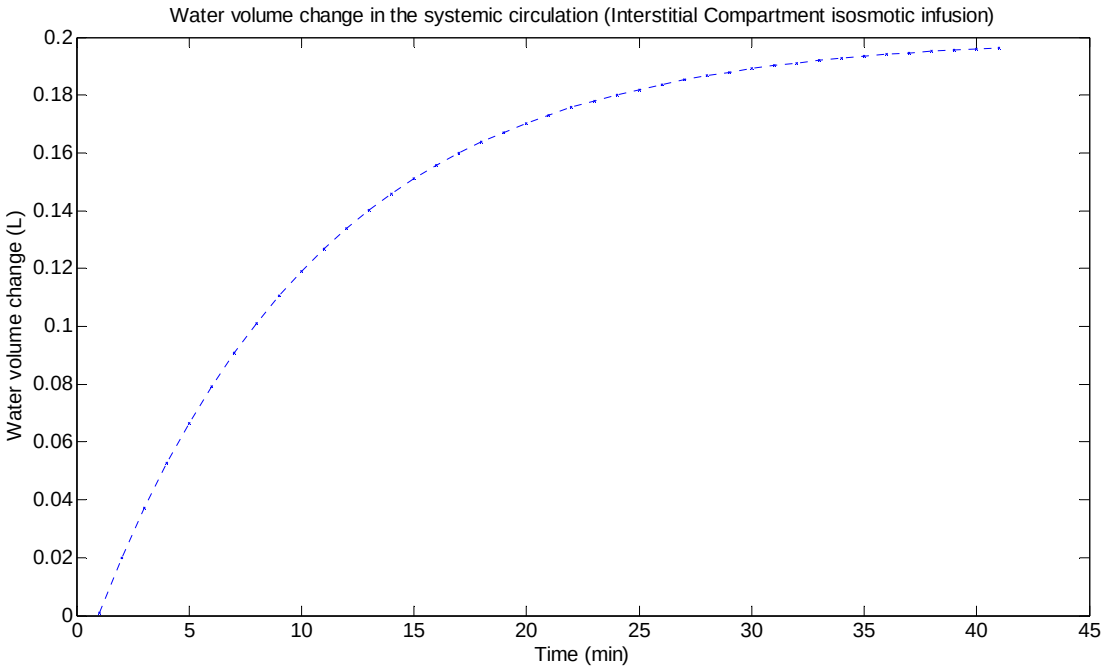

Figure 32 The blood interstitial compartment. The initial portions of the graph correspond to the infusion of the volume in the system.

Figure 33 represents the plasma volume compartment and the change it represents as well. As we can see from the graph the fluid shift decreases due to the infusion of solution in the system. This happens because after the solution is diluted it loses potency due to the modification of the osmolarity.

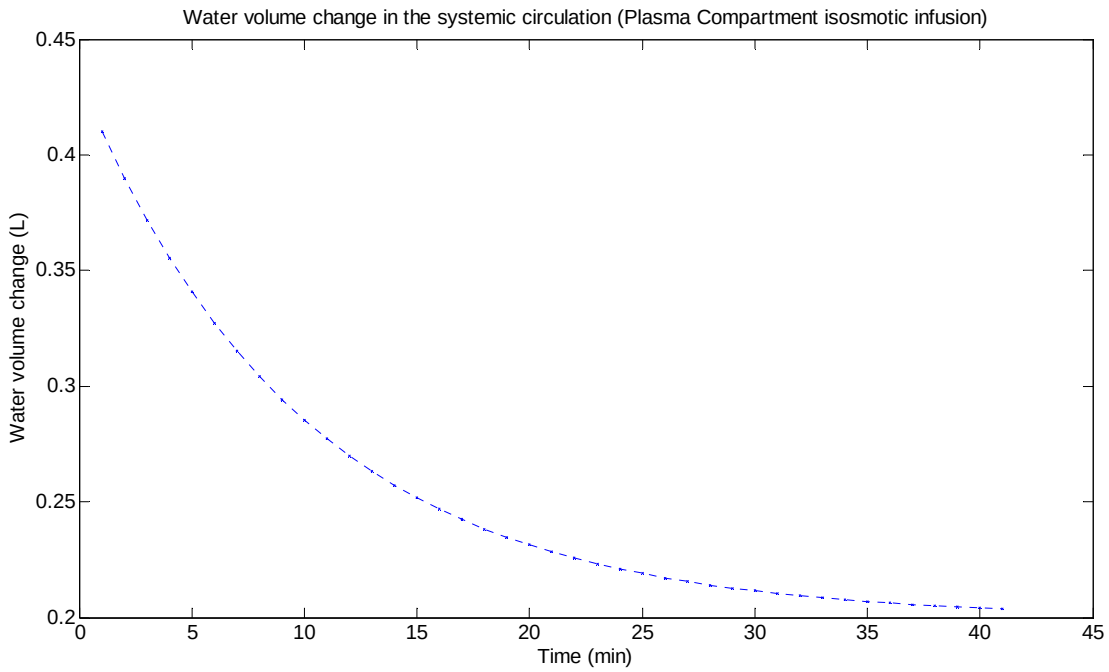

Figure 33 The water volume shifts in the plasma create the movement of solutes in the other compartments. This is because this compartment is the only one with inputs from the system. Then the Starling relationship takes place and allows seepage of fluid through the system.

Salt treatments affect the vasculature in ways that have been mentioned previously. The salt concentrations generate a larger volume change and this is how edema and the influx of fluid get relieved. There is a predicted response since the water that fluxes into the vessels does not follow regular patterns. In the case of the intracranial cavity, the skull restricts the volume change, and therefore unlike the systemic models there is a volume change that has a limit; the limit in our case is the upper bound that the size of the skull can enclose which varies slightly with a change of Young's modulus as a result of the salt concentrations.

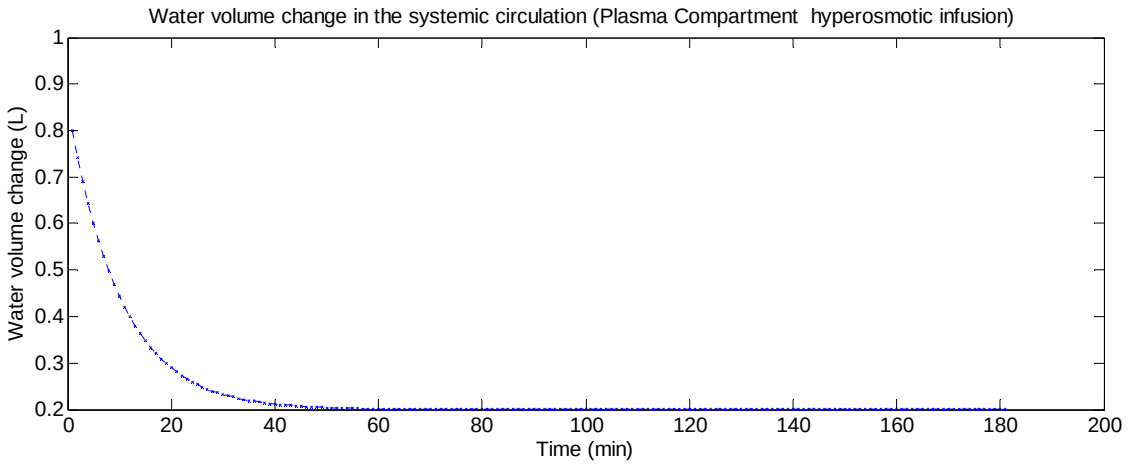

Figure 34 In this graph we can see the difference that happens when there is a hyperosmotic concentration in the compartments. This instance is considered to start after the previous case. Therefore the shift starts at 0.2 L.

4.6. Intracranial pressure and the skull

Intracranial pressure follows the same dynamics that are depicted in Figure 34, but the skull is an upper bound limit. The skull also creates additional tension in the tissues that cause extra damage, which can increase the pressure inside of the cavity. In Table 14 we can see the effect on the pressure due to the hypertonic and normal saline embedded in the system. In this high pressure instance, the salt effect in the skull can have a great impact in the overall dynamics of the system.

From these results it can also be hypothesized that the skull can absorb the salts and therefore restrict the therapy potency even further in those instances in which the therapy ceases to work (after several hours of treatment). Furthermore, it can be seen that the tension increases as the brain radius decreases (more tension towards the

ventricles). The morphology of the brain includes the gray matter, the white matter and the ventricles.

Table 14 Intracranial tension results at 100 mm Hg (0.004 trimmed mean samples).

Condition	Tension at the white matter	Tension at the gray matter
DPBS	120 ± 90	29 ± 7
hDPBS	147 ± 84	35 ± 20

CHAPTER V

CONCLUSIONS AND FUTURE RECOMMENDATIONS

This research investigated the impact that saline solutions have on the skull. We were able to successfully establish that there is a statistical difference in the Young's modulus of bone that was treated when comparing to treatment with solutions of different ion strengths. Below is the summary of the research results.

5.1. Main findings

5.1.1. Bone mechanical testing

After the onset of intracranial hypertension in TBI, patients experience inflammatory responses and other secondary pathways that can worsen the prognosis of the patient. Hypertonic saline solutions are one of the recommended treatments to relieve these effects. Therefore, we tested the premise that bone gets affected by the treatment of these solutions when compared to the control which is water.

Testing and analyzing of the mechanical properties of bone had to follow a special framework. It was determined by visual inspection (microscopy) that the bone has porosity. Because of the porosity of the material, and because it did not behave following Hooke's law, we concluded the material was a cellular solid. The material appear to behave like a cellular solid because of the porosity, unit structure, and theory (Dr. Gibson has stated that bone is a cellular solid (26)). The cellular solids theory states that the materials with high porosity have three prearranged regions: a liner elastic

region, a plateau region, and a densification region. We could see that these regions were present in the analysis of bone.

The Young's modulus analysis yielded high statistical difference when two solutions were compared (DI, hDPBS) in different cross head conditions (0.02, 0.004, 0.002 (mm/s)). This test was performed to see if the solution affected the behavior when compared to the cross head speed, a measurement factor that is can influence the mechanical properties of bone.

The factorial test described in the previous paragraph yielded a statistical difference of less than p=0.001 for a Ho that the means are equal. The specific pairs in the comparison that yielded a p-value ≤ 0.05 were the following for this test: DI 0.02 (mm/s) vs. DI 0.002 (mm/s), DI 0.004 (mm/s) vs. DI 0.002 (mm/s), DI 0.02 (mm/s) vs. hDPBS 0.02 (mm/s), DI 0.02 (mm/s) vs. hDPBS 0.002 (mm/s), DI 0.02 (mm/s) vs. hDPBS 0.004 (mm/s), DI 0.004 (mm/s) vs. hDPBS 0.02 (mm/s) and DI 0.004 (mm/s) vs. hDPBS 0.002 (mm/s). This information was set up in Table 4.

This shows that the strain rates yield statistically different results because there is a difference among the DI samples tested with different cross head speed, and a difference among DI and hDPBS samples. For the samples prepared with hDPBS, it was found that there was no statistical difference found among the cross head speeds tested when compared to each other.

5.1.2. Modeling of solutions

Traumatic Brain Injury is a major cause of death in the United States and the healing methodologies are gravely ineffective. Additionally it is very difficult to study an

organism as a whole involving all of the components, so mathematical modeling for this condition is one of the most feasible choices for its study.

When modeling the solutions in the intracranial cavity current models were used. The model was based on the Guyton, Wolf, and Gyene main equations, although additional equations from other authors were also used (Table 10). The main additions to the current models were three: 1) the involvement of pulsatile flow creation; 2) the inclusion of continuum principles when modeling the behavior of the vessel; and 3) the inclusion of the bone input in the model.

We can see that sinusoidal movement of the vascular fluid in the brain allows for the creation of the CSF and that the information plotted can be related to other published results (Figure 30). Elastic constants can be better modeled by the use of constitutive relationships of bio-material characteristics than by empirical relationships. Plasma shifts are similar in the intracranial cavity that in the overall system.

Taking the inclusion of the bone input into the model, we find that the tension in the skull increases with decreasing radius, and that the salt concentration modifies the skull properties in a very small scale. But this minimal change can have a large impact when the changes in pressure are large and towards the ventricles Table 15.

Table 15 Intracranial tension results.

Condition	Tension at the white matter (mmHg)	Tension at the gray matter (mmHg)
DPBS	120 ± 90	29 ± 7
hDPBS	147 ± 84	35 ± 20

5.2. Recommendations for future research

Pericardial swine xenograft heart valves have been successfully used to supplant human heart valves. They provide advantages over man-made materials, and part of their efficiency relies on the valve treatment which destroys the cells and protein present; therefore it does not cause adverse biological reactions.

Bone marrow functions as a hematopoetic source; its properties are beyond the regulation of bone mechanics. Bone implants should consider this aspect more deeply. Swine bone could theoretically be used as skull replacement for excised pieces. The compressive strength of the human skull is 73MPa, and that of swine is 50MPa. Bone is also a more advantageous structure to undergo denatured treatments, and because the majority of the strength of bone relies on its matrix this could be a successful application of xenotransplant.

In regards to the model created, the modeling of new treatments was an important factor taken into account when the code was created. Current treatments are very inadequate and there needs to be a framework that is easy to use, reliable, and that involves current information in which new hypotheses can be tested.

REFERENCES

1. Doyle JA, Davis DP, Hoyt DB. 2001. The use of Hypertonic Saline in the Treatment of Traumatic Brain Injury. *J. Trauma* 50:367-83

2. Wolf MB. 1982. Estimation of Whole-Body Capillary Transport Parameters from Osmotic Transient Data. *Am. J. Physiol.* 242:R227-R36

3. Sherwood L. 2008. *Human Physiology: From Cells to Systems*. pp 1-16, 510, 303. Belmont, CA.: Cengage Learning

4. Silverthorn DU. 2004. *Human Physiology: An Integrated Approach*. pp 64-65, 490-655. San Francisco, CA.: Pearson

5. Seifter J, Sloane D, Ratner A. 2005. *Concepts in Medical Physiology*. pp 128. Philadelphia, PA.: Lippincott Williams & Wilkins

6. Miller JT, O'Rourke RA, Crawford MH. 1988. Left Atrial Enlargement: An Early Sign of Hypertensive Heart Disease. *Am. Heart J.* 116:1048-51

7. Kaufman B, Weiss MH, Young HF, Nulsen FE. 1973. Effects of Prolonged Cerebrospinal Fluid Shunting on the Skull and Brain. *J. Neurosurg.* 38:288

8. Park JB, Lakes RS. 1992. *Biomaterials: An Introduction*. pp 223-244. New York.: Springer

9. Sherwood ER, Toliver-Kinsky T. 2004. Mechanisms of the Inflammatory Response. *Best Pract. Res. Clin. Anaesthesiol.* 18:385-405

10. Hensley K, Floyd RA, Zheng N, Nael R, Robinson KA, et al. 1999. p38 Kinase is Activated in the Alzheimer's Disease Brain. *J. Neurochem.* 72:2053-8

11. Reid-Arndt SA, Johnstone B. 2009. *The Brain Injury Guide and Resources*. http://braininjuryeducation.org

12. IBISSgroup. 2009. *Traumatic Brain Injury*. http://www.slavicabiochem.com/

13. Merrick MA. 2002. Secondary Injury After Musculoskeletal Trauma: A Review and Update. *J. Athl. Train.* 37:209-17

14. Granacher RP. 2007. *Traumatic Brain Injury: Methods for Clinical and Forensic Neuropsychiatric Assessment*. pp 1-47. Boca Raton, FL.: CRC Press

15. Ghajar J. 2000. Traumatic Brain Injury. *Lancet* 356:923-9

16. Miller JD, Becker DP, Ward JD, Sullivan HG, Adams WE, Rosner MJ. 1977. Significance of Intracranial Hypertension in Severe Head Injury. *J. Neurosurg.* 47:503-16

17. Juul N, Morris GF, Marshall SB, Marshall LF, Trial ECIS. 2000. Intracranial Hypertension and Cerebral Perfusion Pressure: Influence on Neurological Deterioration and Outcome in Severe Head Injury. *J. Neurosurg.* 92:1-6

18. Harutjunyan L, Holz C, Rieger A, Menzel M, Grond S, Soukup J. 2005. Efficiency of 7.2% Hypertonic Saline Hydroxyethyl Starch 200/0.5 Versus Mannitol 15% in the Treatment of Increased Intracranial Pressure in Neurosurgical Patients - A Randomized Clinical Trial [Isrctn62699180]. *Crit. Care* 9:R530-R40

19. Fraser RT, Clemmons DC. 2000. *Traumatic Brain Injury Rehabilitation: Practical Vocational, Neuropsychological, and Psychotherapy Interventions*. pp 16. Danvers, MA.: CRC Press LLC

20. Viano DC. 1989. *Biomechanics of Head Injury-Toward a Theory Linking Head Dynamic Motion, Brain Tissue Deformation and Neural Trauma*. http://papers.sae.org/881708

21. Lind NM, Moustgaard A, Jelsing J, Vajta G, Cumming P, Hansen AK. 2007. The Use of Pigs in Neuroscience: Modeling Brain Disorders. *Neurosci Biobehav R* 31:728-51

22. Lescot T, Abdennour L, Boch AL, Puybasset L. 2008. Treatment of Intracranial Hypertension. *Curr. Opin. Crit. Care.* 14:129-34

23. Gyenge CC, Bowen BD, Reed RK, Bert JL. 1999. Transport of Fluid and Solutes in the Body I. Formulation of a Mathematical Model. *Am. J. Physiol. Heart. Circ. Physiol.* 277:H1215-H27

24. Gyenge CC, Bowen BD, Reed RK, Bert JL. 1999. Transport of Fluid and Solutes in the Body II. Model Validation and Implications. *Am. J. Physiol. Heart. Circ. Physiol.* 277:H1228-H40

25. Huh K-H, Yi W-J, Jeon I-S, Heo M-S, Lee S-S, et al. 2006. Relationship Between Two-Dimensional and Three-Dimensional Bone Architecture in Predicting the Mechanical Strength of the Pig Mandible. *Oral Surg. Oral Med. Oral Pathol. Oral Radiol. Endod.* 101:363-73

26. Gibson LJ, Ashby MF. 1999. *Cellular Solids: Structure and Properties*. Melbourne, AU. : Cambridge University Press

27. Turner CH, Chandran A, Pidaparti RMV. 1995. The Anisotropy of Osteonal Bone and Its Ultrastructural Implications. *Bone* 17:85-9

28. An YH, Barfield WR, Bensen CV, Bonucci E, Draughn RA, et al. 2000. *Mechanical Testing of Bone and the Bone-Implant Interface*. pp 3-151. Boca Raton, FL.: CRC Press LLC

29. Gibson LJ. 2005. Biomechanics of Cellular Solids. *J. Biomech.* 38:377-99

30. Ashby MF. 2006. The Properties of Foams and Lattices. *Philos. T. Roy. Soc. A.* 364:15-30

31. Pampolini G, Del Piero G. 2009. Strain Localization in Polyurethane Foams: Experiments and Theoretical Model. *J.O.M.M.S.* 3:29-38

32. Hård af Segerstad P, Toll S. 2008. Open-Cell Cellular Solids: A Constitutive Equation for Hyperelasticity with Deformation Induced Anisotropy. *Int. J. Solid Struct.* 45:1978-92

33. Scott AS, Fong E. 2009. *Body Structures and Functions*. pp 92-121. Clifton Park, NY.: Cengage Learning

34. Boskey AL, Burr DB, Cowin SC, Dieudonné SC, Jee WSS, et al. 2003. *Bone Mechanics Handbook*. pp Ch 1,7. Boca Raton, FL.: CRC Press LLC

35. Chiras DD. 2010. *Human Biology*. pp 75-76. Sudbury, MA.: Jones & Bartlett Learning

36. Cowin SC, Hegedus DH. 1976. Bone Remodeling I. Theory of Adaptive Elasticity. *J. Elasticity* 6:313-26

37. Hegedus DH, Cowin SC. 1976. Bone Remodeling II - Small Strain Adaptive Elasticity. *J. Elasticity* 6:337-52

38. Canalis E, McCarthy T, Centrella M. 1988. Growth Factors and the Regulation of Bone Remodeling. *J. Clin. Invest.* 81:277-81

39. Manolagas SC, Jilka RL. 1995. Bone Marrow, Cytokines, and Bone Remodeling. Emerging Insights into the Pathophysiology of Osteoporosis. *N. Engl. J. Med.* 332:305-11

40. Looker AC, Bauer DC, Chesnut CH, 3rd, Gundberg CM, Hochberg MC, et al. 2000. Clinical Use of Biochemical Markers of Bone Remodeling: Current Status and Future Directions. *Osteoporos. Int.* 11:467-80

41. Perrott DH, Rahn B, Wahl D, Linke B, Thurüller P, et al. 2003. Development of a Mechanical Testing System for a Mandibular Distraction Wound. *Int. J. Oral Maxillofac. Surg.* 32:523-7

42. Chehade MJ, Pohl AP, Pearcy MJ, Nawana N. 1997. Clinical Implications of Stiffness and Strength Changes in Fracture Healing. *J Bone Joint Surg Br* 79B:9-12

43. Cope JB, Samchukov ML. 2001. Mineralization Dynamics of Regenerate Bone During Mandibular Osteodistraction. *Int J Oral Max Surg* 30:234-42

44. Aarnes GT, Steen H, Ludvigsen P, Kristiansen LP, Reikeras O. 2002. High Frequency Distraction Improves Tissue Adaptation During Leg Lengthening in Humans. *J. Orthop. Res.* 20:789-92

45. Ilizarov GA. 1989. The Tension Stress Effect on the Genesis and Growth of Tissues II. The Influence of the Rate and Frequency of Distraction. *Clin Orthop Relat R* 239:263-85

46. Weinans H, Huiskes R, Grootenboer HJ. 1992. The Behavior of Adaptive Bone-Remodeling Simulation Models. *J. Biomech.* 25:1425-41

47. Mosekilde L, Kragstrup J, Richards A. 1987. Compressive Strength, Ash Weight, and Volume of Vertebral Trabecular Bone in Experimental Fluorosis in Pigs. *Calcified Tissue Int* 40:318-22

48. Lalande A, Roux C, Graulet A-M, Schiavi P, De Vernejoul M-C. 1998. The Diuretic Indapamide Increases Bone Mass and Decreases Bone Resorption in Spontaneously Hypertensive Rats Supplemented with Sodium. *J. Bone Miner. Res.* 13:1444-50

49. Massey LK, Whiting SJ. 1996. Dietary Salt, Urinary Calcium, and Bone Loss. *J. Bone. Miner. Res.* 11:731-6

50. Carter DR, Hayes VC. 1977. The Compressive Behavior of Bone as a Two-Phase Porous Structure. *J. Bone Joint. Surg. Am.* 59:954-62

51. Linde F, Norgaard P, Hvid I, Odgaard A, Soballe K. 1991. Mechanical-Properties of Trabecular Bone - Dependency on Strain Rate. *J. Biomech.* 24:803-9

52. Humphrey JD. 2002. *Cardiovascular Solid Mechanics: Cells, Tissues, and Organs*. pp 249-364. New York: Springer-Verlag

53. Giddings VL, Kurtz SM, Jewett CW, Foulds JR, Edidin AA. 2001. A Small Punch Test Technique for Characterizing the Elastic Modulus and Fracture Behavior of PMMA Bone Cement Used in Total Joint Replacement. *Biomaterials* 22:1875-81

54. Pompe W, Worch H, Epple M, Friess W, Gelinsky M, et al. 2003. Functionally Graded Materials for Biomedical Applications. *Mater. Sci. Eng.* **362**:40-60

55. Kurtz SM, Foulds JR, Jewett CW, Srivastav S, Edidin AA. 1997. Validation of a Small Punch Testing Technique to Characterize the Mechanical Behaviour of Ultra-High-Molecular-Weight Polyethylene. *Biomaterials* 18:1659-63

56. Onck PR, Andrews EW, Gibson LJ. 2001. Size Effects in Ductile Cellular Solids. Part I: Modeling. *Int. J. Mech. Sci.* 43:681-99

57. FDA. 2008. *Animal Models — Essential Elements to Address Efficacy Under the Animal Rule*. http://www.fda.gov/downloads/Drugs/GuidanceComplianceRegulatoryInformation/Guidances/ucm072214.pdf

58. Hughes HC. 1986. Swine in Cardiovascular Research. *Lab. Anim. Sci.* 36:348-50

59. Popowics TE, Zhu Z, Herring SW. 2002. Mechanical Properties of the Periosteum in the Pig, *Sus scrofa*. *Arch. Oral Biol.* 47:733-41

60. Guyton AC. 1965. Interstitial Fluid Pressure: II. Pressure-Volume Curves of Interstitial Space. *Circ. Res.* 16:452-60

61. Guyton AC, Prather J, Scheel K, McGehee J. 1966. Interstitial Fluid Pressure IV. Its Effect on Fluid Movement Through the Capillary Wall. *Circ. Res.* 19:1022-30

62. Guyton AC, Scheel K, Murphree D. 1966. Interstitial Fluid Pressure III. Its Effect On Resistance To Tissue Fluid Mobility. *Circ. Res.* 19:412-9

63. Wolf MB. 1975. Estimation of Parameters Affecting Rapid Fluid Transfers in the Whole Body. I. Isotonic Infusions. *Ann. Biomed. Eng.* 3:209-24

64. Abbott NJ. 2004. Evidence for Bulk Flow of Brain Interstitial Fluid: Significance for Physiology and Pathology. *Neurochem. Int.* 45:545-52

65. McCarthy T. 1997. *Animal Models in Medical Device Development and Qualification*. http://www.criver.com/sitecollectiondocuments/rm_rm_r_animal_models_med_device.pdf

66. Wang S, Liu Y, Fang D, Shi S. 2007. The Miniature Pig: A Useful Large Animal Model for Dental and Orofacial Research. *Oral Dis.* 13:530-7

67. Teo JCM, Si-Hoe KM, Keh JEL, Teoh SH. 2007. Correlation of Cancellous Bone Microarchitectural Parameters from MicroCT to CT Number and Bone Mechanical Properties. *Mater. Sci. Eng. C.* 27:333-9

68. Mao X, Hideaki T. 1987. Development of a Further- Miniaturized Specimen of 3 mm Diameter for Tem Disk (ø 3 mm) Small Punch Tests. *J. Nucl. Mater.* 150:42-52

69. Riester L, Ferber MK, Breder K, Bridge RJ. 1997. *Elastic Modulus Calculations from Load/Displacement Curves Using Spherical and Pointed Indenters*. http://www.osti.gov/bridge/purl.cover.jsp?purl=/521607-m1qCno/webviewable/

70. Montgomery DC, Runger GC. 2006. *Applied Statistics and Probability for Engineers* Danvers, MA.: John Wiley & Sons Inc. 121, 229-34 pp.

71. Andrews EW, Gioux G, Onck P, Gibson LJ. 2001. Size Effects in Ductile Cellular Solids. Part II: Experimental Results. *Int. J. Mech. Sci.* 43:701-13

72. Teo JCM, Si-Hoe KM, Keh JEL, Teoh SH. 2006. Relationship Between CT Intensity, Micro-Architecture and Mechanical Properties of Porcine Vertebral Cancellous Bone. *Clin. Biomech.* 21:235-44

73. Fenech CM, Keaveny TM. 1999. A Cellular Solid Criterion for Predicting the Axial-Shear Failure Properties of Bovine Trabecular Bone. *J. Biomech Eng.-T. ASME* 121:414-22

74. Kotha SP, Walsh WR, Pan Y, Guzelsu N. 1998. Varying the Mechanical Properties of Bone Tissue by Changing the Amount of its Structurally Effective Bone Mineral Content. *Bio-Med. Mater. Eng.* 8:321-34

75. Bandyopadhyay U, Basu A, Bhattacharya R, Biswas A, Chakraborty H, et al. 2008. *Statistical Advances In the Biomedical Sciences: Clinical Trials, Epidemiology, Survival Analysis, and Bioinformatics*. pp 501-526. Hoboken, NJ.: Wiley-Interscience

76. Wilsea M, Johnson KL, Ashby MF. 1975. Indentation of Foamed Plastics. *Int. J. Mech. Sci.* 17:457-60

77. Clemens P. 2007. *Traumatic Brain Injury: Management on the Neurointensive Care Unit*. http://www.frca.co.uk/article.aspx?articleid=100913

78. Maas AI, Fleckenstein W, de Jong DA, van Santbrink H. 1993. Monitoring Cerebral Oxygenation: Experimental Studies and Preliminary Clinical Results of Continuous Monitoring of Cerebrospinal Fluid and Brain Tissue Oxygen Tension. *Acta Neurochir. Suppl. (Wien)* 59:50-7

79. Czosnyka M, Pickard JD. 2004. Monitoring and Interpretation of Intracranial Pressure. *J. Neurol. Neurosur. Ps.* 75:813-21

80. Cudd TA, Purinton S, Patel NC, Wood CE. 1998. Cardiovascular, Adrenocorticotropin, and Cortisol Responses to Hypertonic Saline in Euvolemic Sheep are Altered by Prostaglandin Synthase Inhibition. *Shock* 10:32-6

81. Dubick MA, Davis JM, Myers T, Wade CE, Kramer GC. 1995. Dose Response Effects of Hypertonic Saline and Dextran on Cardiovascular Responses and Plasma Volume Expansion in Sheep. *Shock* 3:137-44

82. Pascual JM, Watson JC, Runyon AE, Wade CE, Kramer GC. 1992. Resuscitation of Intraoperative Hypovolemia: A Comparison of Normal Saline and Hyperosmotic/Hyperoncotic Solutions in Swine. *Crit. Care Med.* 20:200-10

83. Adrogué HJ, Madias NE. 2000. Hypernatremia. *New Engl. J. Med.* 342:1493-9

84. Jennett B, Bond M. 1975. Assessment of Outcome After Severe Brain Damage. *The Lancet* 1:480-4

85. Becker DP, Miller JD, Ward JD, Greenberg RP, Young HF, Sakalas R. 1977. The Outcome from Severe Head Injury with Early Diagnosis and Intensive Management. *J. Neurosurg.* 47:491-502

86. Kelly DF, Gonzalo ITG, Cohan P, Berman N, Swerdloff R, Wang C. 2000. Hypopituitarism Following Traumatic Brain Injury and Aneurysmal Subarachnoid Hemorrhage: A Preliminary Report. *J. Neurosurg.* 93:743-52

87. Agha A, Rogers B, Sherlock M, O'Kelly P, Tormey W, et al. 2004. Anterior Pituitary Dysfunction in Survivors of Traumatic Brain Injury. *Clin. Endocrinol.* 89:4929-36

88. Lenzlinger PM, Morganti-Kossmann M-C, Laurer HL, McIntosh TK. 2001. The Duality of the Inflammatory Response to Traumatic Brain Injury. *Mol. Neurobiol.* 24:169-81

89. Froelich M, Härtl R. 2008. Ultra-Early Hyperosmolar Treatment in Traumatic Brain Injury: Will Surgery Soon be Old-School? *Crit. Care Med.* 36:642

90. Morganti-Kossmann M-C, Satgunaseelan L, Bye N, Kossmann T. 2007. Modulation of Immune Response by Head Injury. *Injury* 38:1392-400

91. Griffin L. 2010. *Hypertonic Saline in the Treatment of Intracranial Hypertension*. http://www.ispub.com/journal/the_internet_journal_of_advanced_nursing_practice/

92. Bullock MR, Chesnut R, Ghajar J, Gordon D, Hartl R, et al. 2006. Surgical Management of Acute Epidural Hematomas. *Clin. Neurol. Neurosur.* 58:S2.7-S2.15

93. Ramming S, Shackford SR, Zhuang J, Schmoker JD. 1994. The Relationship of Fluid Balance and Sodium Administration to Cerebral Edema Formation and Intracranial Pressure in a Porcine Model of Brain Injury. *J. Trauma* 37:705-13

94. Levine JM. 2006. Hypertonic Saline for the Treatment of Intracranial Hypertension: Worth its Salt. *Crit. Care Med.* 34:3037-9

95. Wisner DH, Schuster L, Quinn C. 1990. Hypertonic Saline Resuscitation of Head Injury: Effects on Cerebral Water Content. *J. Trauma* 30:75-8

96. Qureshi AI, Suarez JI. 2000. Use of Hypertonic Saline Solutions in Treatment of Cerebral Edema and Intracranial Hypertension. *Crit. Care Med.* 28:3301-13

97. Guyot LL, Michael DB. 2000. Post-Traumatic Hydrocephalus. *Neurol. Res.* 22:25-8

98. Shapiro K, Fried A, Takei F, Kohn I. 1985. Effect of the Skull and Dura on Neural Axis Pressure-Volume Relationships and CSF Hydrodynamics. *J. Neurosurg.* 63:76-81

99. Pullen RG, DePasquale M, Cserr HF. 1987. Bulk Flow of Cerebrospinal Fluid into Brain in Response to Acute Hyperosmolality. *Am. J. Physiol.* 253:F538-F45

100. Reulen HJ, Graham R, Spatz M, Klatzo I. 1977. Role of Pressure Gradients and Bulk Flow in Dynamics of Vasogenic Brain Edema. *J. Neurosurg.* 46:24-35

101. Rosenberg GA, Wolfson LI, Katzman R. 1978. Pressure- Dependent Bulk Flow of Cerebrospinal Fluid into Brain. *Exp. Neurol.* 60:267-76

102. Rosenberg GA, Kyner WT, Estrada E. 1980. Bulk Flow of Brain Interstitial Fluid Under Normal and Hyperosmolar Conditions. *Am. J. Physiol.* 238:F42-F9

103. Greitz D, Franck A, Nordell B. 1993. On the Pulsatile Nature of Intracranial and Spinal CSF-Circulation Demonstrated by MR Imaging. *Acta Radiol.* 34:321-8

104. Chandran KB, Yoganathan AP, Rittgers SE. 2007. *Biofluid Mechanics: The Human Circulation*. pp 195-221. Boca Raton, FL.: CRC Press Taylor and Francis Group

105. Takamizawa K, Hayashi K. 1987. Strain Energy Density Function and Uniform Strain Hypothesis for Arterial Mechanics. *J. Biomech.* 20:7-17

106. He X, Ku DN, Moore JE, Jr. 1993. Simple Calculation of the Velocity Profiles for Pulsatile Flow in a Blood Vessel Using Mathematica. *Ann. Biomed. Eng.* 21:45-9

107. Moore JE, Jr., Ku DN. 1994. Pulsatile Velocity Measurements in a Model of the Human Abdominal Aorta Under Resting Conditions. *J. Biomech. Eng.* 116:337-46

108. Ursino M, Ter Minassian A, Lodi CA, Beydon L. 2000. Cerebral Hemodynamics During Arterial and CO_2 Pressure Changes: In Vivo Prediction by a Mathematical Model. *Am. J. Physiol. Heart Circ. Physiol.* 279:H2439-H55

109. Kimelberg HK. 2004. Water Homeostasis in the Brain: Basic Concepts. *Neuroscience* 129:851-60

110. Epstein CM. 1974. The Distribution of Intracranial Forces in Acute and Chronic Hydrocephalus. *J. Neurol. Sci.* 21:171-80

111. del Zoppo GJ, Faraci FM, Feuerstein G, Heistad D, Miller A, et al. 1997. *Primer on Cerebrovascular Diseases*. pp 25-28. San Diego, CA. : Academic Press

VITA

Name:	Mariana Ceballos
Address:	Texas A&M University Department of Mechanical Engineering 3123 TAMU College Station TX 77843-3123
Email Address:	mariana.ceballos@gmail.com
Education:	B.S., Biomedical Engineering, Florida International University, 2007 M.S., Mechanical Engineering, Texas A&M University, 2011